EXAMINATION OF STRUCTURAL, VIBRATIONAL AND ELECTRONICAL PROPERTIES OF p-BENZOPHENONEOXYCARBONYLPHENYL ACRYLATE MOLECULE WITH THE AID OF DENSITY FUNCTIONAL THEORY AND HARTREE-FOCK METHODS

by

FIRAT KARABOĞA

THESIS SUBMITTED TO
THE GRADUATE SCHOOL OF NATURAL AND APPLIED SCIENCES
OF
THE ABANT İZZET BAYSAL UNIVERSITY
IN PARTIAL FULFILLMENT OF THE REQUIREMENTS FOR THE DEGREE OF
MASTER OF SCIENCE
IN
THE DEPARTMENT OF PHYSICS

JANUARY 2013

Approval of the Graduate School of Natural and Applied Science

_____

Prof. Dr. Yaşar DÜRÜST

Director

I certify that this thesis satisfies all the requirements as a thesis for the degree of Master of Science.

Prof. Dr. Cabir TERZİOĞLU

Head of Physics Department

This is to certify that we have read this thesis and that in our opinion it is fully adequate, in scope and quality as a thesis for the degree of Master of Science.

Prof. Dr. Cabir TERZİOĞLU

Advisor

Examining Committee Members:

1. Prof. Dr. Cabir TERZİOĞLU.....

2. Assoc. Prof. Dr. Yusuf ATALAY.....

3. Assoc. Prof. Dr. Cihan PARLAK.....

ABSTRACT

EXAMINATION OF STRUCTURAL, VIBRATIONAL AND ELECTRONICAL PROPERTIES OF p-BENZOPHENONEOXYCARBONYLPHENYL ACRYLATE MOLECULE WITH THE AID OF DENSITY FUNCTIONAL THEORY AND HARTREE-FOCK METHODS

KARABOĞA, Fırat

Master of Science, Department of Physics

Advisor: Prof. Dr. Cabir TERZİOĞLU

January 2013, 93 Pages

The main objective of this thesis is to characterize a title compound, p-benzophenoneoxycarbonylphenyl acrylate (BPOCPA) by means of experimental and theoretical evidences. The spectroscopic properties of the compound are experimentally examined by Fourier transformation-infrared (FTIR) spectra (in the region 400–4000 cm^{-1}), nuclear magnetic resonance (NMR) chemical shifts (with a frequency of 400 MHz), and ultra violet-visible (UV–vis) spectra (in the wavelength range of 400–700 nm). For the theoretical studies, the optimized molecular structures, vibrational frequencies including infrared intensities and Raman activities, corresponding vibrational spectra interpreted with the aid of normal coordinate analysis based on scaled density functional force field, atomic charges,

thermodynamic properties, UV–vis spectra, ^{1}H and ^{13}C NMR chemical shifts of the BPOCPA monomer are analyzed in the ground state with the aid of ab initio Hartree–Fock (HF) and the density functional theory (B3LYP) with the standard 6-311++G(d,p) level of theory for the first time. All the results obtained show that the vibrational frequencies, absorption wavelengths and chemical shifts (especially calculated form DFT/B3LYP) are observed to be in good agreement with the available experimental data. According to the comparison between experimental results and theoretical data, the calculation levels chosen play an important role in understanding of dynamics of the title compound studied in this work. Moreover, not only are the frontier molecular orbitals (highest occupied molecular orbital called as HOMO, and lowest unoccupied molecular orbital named as LUMO), molecular electrostatic potential (MEP) and electrostatic potential (ESP) simulated in detail but the dipole moment, softness, electronegativity, chemical hardness, electrophilicity index, transition state and energy band gap values being responsible for the potential technological and industrial applications are also discussed clearly. Based on the investigations, the BPOCPA molecule with the specific regions is found to be useful to bond metallically and interact intermolecularly. Moreover, the electronegativity, hardness, softness and electrophilicity index calculated demonstrate that the monomer synthesized may be functional in the optic and opto-electronic applications.

Keywords: p-benzophenoneoxycarbonylphenyl acrylate, DFT, HF, MEP and FMO.

ÖZET

YOĞUNLUK FONKSİYONU TEORİSİ VE HARTREE- FOCK METOTLARI YARDIMIYLA, p-BENZOFENONOKSİKARBONİLFENİL AKRİLAT MOLEKÜLÜNÜN YAPISAL, TİTREŞİMSEL VE ELEKTRONİK ÖZELLİKLERİN İNCELENMESİ

KARABOĞA, Fırat

Yüksek Lisans, Fizik Bölümü

Tez Danışmanı: Prof. Dr. Cabir TERZİOĞLU

OCAK 2013, 93 Sayfa

Bu çalışmanın ana konusu, teoriksel ve deneysel veriler sayesinde p-benzofenonoksikarbonilfenil akrilat (BPOCPA) isimli molekülü karakterize etmek. Molekülün spektroskopik özellikleri, deneysel olarak kızılötesi spektrası(400–4000 cm^{-1} aralığında),nükleer manyetik resonans kimyasal kaymaları(400 MHz frekanslı) ve morötesi- görünür bölge spektrası(400-700 nm dalga boyu aralığında) ile incelenir. Teorik çalışmalarda, BPOCPA molekülünün optimize yapıları, ölçeklendirilmiş yoğunluk fonksiyonel kuvvet alanına dayanan normal kordinat analizi aracılığıyla yorumlanan titreşim spektrasıyla ilişkili raman aktifleri ve kızlıötesi yoğunluğu içeren titreşim frekansları, atomic yükler, termodinamik özellikler, morötesi-görünür bölge spectrası, ^{1}H ve ^{13}C nükleer manyetik rezonans kimyasal kaymaları 6-311G++(d,p) temel setli yoğunluk fonksiyonel teorisi (B3LYP) ve

Hartree-Fock yöntemi kullanılarak temel halde ilkkez olarak analiz edilir.Özellikle DFT/B3LYP ile hesaplanmış tüm değerler gösteriyor ki titreşim frekansları, dalga boyu soğurulması ve kimyasal kaymaları uygun deneysel verilerle uyumludur. Deneysel ve teorik sonuçlar arasındaki mukayeseye göre, seçilmiş olan hesaplama seviyesi bu çalışmadaki araştırılan bileşiğin dinamiğini anlamada önemli rol oynar. Bunun dışında, sadece en yüksek eşleşmiş molekül orbitali olarak bilinen HOMO ve en düşük eşleşmemiş molekül orbital olarak bilinen LUMO'yu kapsayan sınır molekül orbitalleri, moleküler elektrostatik potensiyeli ve elektrostatik potensiyeli detaylı gösterilmedi, teknolojik ve endüstriyel uygulamalarıyla ilişkili olan dipol moment, yumuşaklık, elektron alma isteği, kimyasal sertlik, electron verme isteği indeksi, geçiş durumu ve enerji bant aralığı da açıkça tartışılır. Araştırmalara dayanarak, özel bölgeleriyle BPOCPA molekülünün metalik bağ yapması ve öoleküller arası etkileşme için kullanışlı olduğu bulunur. Üstelik, hesaplanılmış olan elektron alma isteği, sertlik, yumuşaklık ve elektron verme isteği indeksi, sentezlenmiş olan monomerin optic ve opto-elektronikte kullanışlı olabileceğini gösteriyor.

Anahtar Kelimeler: p-benzofenonoksikarbonilfenil akrilat, DFT, HF, MEP ve FMO

to my lovely family...

ACKNOWLEDGEMENTS

I would like to thank My Supervisor, Prof. Dr. Cabir TERZİOĞLU for his guidance and support throughout this thesis and also with my professional development.

Special thanks are given to Assist. Prof. Dr. Gürcan YILDIRIM, being always accessible, is willing to help throughout this dissertation. I sent sincere thanks to extend my computational physics vision about use of Gaussian 09 program by means of his lengthy and useful conversations.

I would like to thank my thesis committee members for their guidance and assistance through this process. Of course, their discussion, comments, ideas and especially feedback have certainly been invaluable to interpret and improve the results obtained.

I would also like to thank my research friend Musa DOĞRUER, who is expert of MgB_2 and YusuF ZALAOĞLU for their supports, and help during my research.

I would gratefully like to extend my sincere thanks to, Uğur SOYKAN who is the master of polymer chemistry, Ali Yiğit KUTLUCA, Mehmet AVCI and Salih SEKİTMEN who act as my brother all parts of my life.

I am very grateful to my amazing parents: Mom, Dad, Brother and Sisters for their love, moral support, constant encouragement, and prayers throughout this process.

TABLE OF CONTENTS

LIST OF TABLES

LIST OF FIGURES

CHAPTER 1

INTRODUCTION

The study of liquid crystals began in 1888 when an Austrian botanist named Friedrich Reinitzer observed that a material known as cholesteryl benzoate had two distinct melting points. Liquid crystal materials generally have several remarkable characteristics. Liquid crystals (LCs) have a good reputation for their inherent self assembly, rich phase behaviour and diverse anisotropic properties [1-5].In this aspect, liquid crystalline polymers (LCPs) being a kind of polymer that indicates liquid crystal phases can be utilized to provide effective mechanical properties to polymer with the help of their backbone orientation seen explicitly when external force is applied. They also have various application areas such as in electronic devices extensively in screen technology, improving desired optical, thermal properties and processing characteristics [6-8].In addition, Side-chain liquid-crystalline polymers (SCLCPs) represent a combination of liquid- crystalline behavior, and polymeric properties have been the subject of intensive research during the last decades and the molecule(SCLCP), p-benzophenoneoxycarbonylphenyl acrylate, reported to act as liquid crystal can be used mainly with this goal in polymers produced by either main or side grafting method. As a consequence, it has importance at this point to analyze p-benzophenoneoxycarbonylphenyl acrylate via computational methods for lighting future studies used title compound. Moreover, the scientists are forced out to utilize computational methods which are reliable to characterize the molecule because of their efficiency and accuracy with respect to the

evaluation of a number of molecular properties [9].

A suitable quantum chemical study is remarkably preferable to predict compound properties economically, to clarify some experiment phenomena insightfully and to identify the molecule spectroscopy [10]. Because of this reason, the computational researches tend to increase continuously as providing reliability and easier processing [11-13].The methods, DFT (Density Functional Theory), which utilize electron probability density instead of wave functions, and HF (Hartree-Fock), which based on effective potential for electrons' interactions, are indispensible for computational advance based on quantum mechanics without any empirical parameters, hence the vibrational frequencies, ^{1}H and ^{13}C NMR chemical shifts, UV–Vis spectra, PED analysis, thermodynamic properties and atomic charges were computed the molecular structures by use of B3LYP/6-311++G(d,p), which a branch of DFT methods given minimum energy of the tackling compound and HF/6-311++G(d,p) basis sets. The correlation coefficient between was them determined.

The vibrational frequencies and the chemical shifts results obtained from experiment were found to be good aggrement with theoretical predictions. Collation for theoretical and experimental data revealed that the correlation confirming the responsibility of the methods as well as the frontier orbitals and the molecular electrostatic potential were envisioned before transition states and energy band gaps were determined and interpreted. Thermodynamic properties were investigated mentioned molecule.

The aim of this study is to not only analyze the coherence between theoretical data and experimental values but also illuminate the characterization of p-benzophenoneoxycarbonylphenyl acrylate and lead the way to future studies of this molecule.

CHAPTER 2

COMPUTATIONAL MOLECULE ANALYSIS

2.1. Calculations Types for Multiple-Electron Systems

The detailed information is obtained only for the single-electron system (Hydrogen) by solving completely Schrödinger equation. However, when the number of electrons increases, the exact solution of the schrödinger equation will be more difficult and sophisticate. The exact results are achieved for the energy levels and wave functions of two-electron atom (He) by calculating variation, so some approximations are requested to solve the Schrödinger equation.

The working area of physics is sorted theoretical physics, experimental physics and computational physics. The study of this thesis is computational physics which apply the mathematically methods improved by theoretical physicists and interpret the obtained results by relating between the theoretical and experimental physics. The information is attained for the molecules producing very difficult by means of observation or experimental. This fore-information (qualitative or quantitative results) before any experiments guides to researcher experimental.

There are main two computational methods backing up the computational physicists to support experimental studies and to predict the results obtained before the experimental study such as Molecular Mechanic Method(MM) and Electronic Characteristic Method(ECM) making up from semi-emprical method and ab-initio method.

2.1.1. Molecular Mechanic Method

MM which was improved out of a request to define molecular structures and properties in as practical a manner as possible is based on the Born-Openheimer approximation [14] and the model in which interactions within a system includes stretching of bonds, opening and closing of angles and rotation of single bonds, non bonded interactions (van der waals) etc…The set of potential functions which is derived from the displacement of atoms (empirical set of equations) is named as the probe field which contains adjustable parameter that are accommodated to obtain the most convenient of calculated and experimental properties of the molecules.

$$E_T = E_{streching} + E_{bending} + E_{rotational} + E_{nonbonding} + E \ldots\ldots etc \quad (1)$$

The range of applicability of molecular mechanics (force field) techniques is the molecules containing thousands of atoms, organics, oligonucleotides, peptides, saccharides (metallo-organics and inorganics in some cases) and especially proteins as well as vacuum, implicit, explicit solvent environments, ground state only, thermodynamic and kinetic features. On the other hand, a situation being a handicap for the utilized of force field methods is in effect certain problems are essentially electronic in earth. By construction any property related to the electronic structure for instance electrical conductivity, optical and magnetic properties are not within reach from force field calculations [15] and this method can not of course provide properties that are based on distribution of electrons in a molecule. Since force field methods (MM) neglect electrons' motions and calculate the energy of a system as a function of nuclear position only. Lastly, The Amber, Charmm and Hyberchem are specially programmes for that method [16].

2.1.2. Electronic Characteristic Method

The source calculation of the electronic structure bases on the quantum mechanic laws. When the electronic structure is searched, the mathematical variations are needed for the solution. There are two type methods such as semi-emprical and Ab-initio method.

2.1.2.1. Semi-Emprical Method

In this method, excessively experimental parameters are used to calculate easier the molecule properties, so the calculation time is shorter than Ab-initio method. The working princible of this method is the same for the beginning with Hartree-Fock method but it uses experimental parameters to solve roughly the schrödinger equation. Moreover, core orbitals are steady since they don't alter relatively in chemical reactions and a minimum set of valence orbitals is conceived only on each carbon (2s, $2p_x$, $2p_y$, $2p_z$ on carbon). Some semi-emprical methods are CNDO, INDO MINDO, ZINDO, PM3 (parametric model) and AM1 (Austin model).

2.1.2.2. Ab-Initio Method

Ab-initio means "from beginning" in Latin. While the schrödinger equation is solved, any experimental data are not used excluding physical quantities such as the mass of electron, the speed of light etc... in this method which bases on quantum mechanics. This method includes different types of the calculations. They are Hartree-Fock (HF), Density Functional Theory(DFT), The Møller-Plesset Perturbation Theory(MP) and Configuration Interaction(CI).The only difference between these calculations is the electron correlation which is not considered in HF

method and is regarded in others methods. The Ab-initio methods are more accurate but much slower than semi-emprical method. Furthermore, By using the Ab-initio method;

* geometry optimizations,

* electronic structure

* frequency calculations,

* transition structures and reaction paths,

* charge distributions of electrons,

* potential energy surfaces (PES),

* rate constants for chemical reactions

* NMR, FTIR, RAMAN and UV spectroscopies

* thermodynamic calculations- heat of reactions, energy of activation

*balk physical and chemical properties of molecules can be studied theoretically in computational chemistry[17].

In last, GAUSSIAN, GAMESS, HYPERCHEM, CACHE etc... are the package programmes in the use of Ab-initio method [18].

2.2. Hartree-Fock (HF) Method

In accordance with Hartree-Fock(HF) model, each electron in systems containing defined-number electrons moves in effective potential that is relevant to average field of coulomb interactions caused by existence of remaining electrons and attractive force of nucleus [19].In conclusion that Hartree approximation is based on writing many-electron system's wave function as a product of a single electron wave functions [20]. Initially, One can begin the Hartree-Fock process for a Helium, has

two electrons, by creating two-electron wave function like that;

$$\Psi(r_1, r_2) = \Psi(r_1)\ \Psi(r_2) \tag{2}$$

Since assumed that both electrons are in the same orbital in according to Pauli exclusion pricible, in equation (2) on the right side wave functions are same. The based on the equation (2), $\Psi^*(r_2)\ \Psi(r_2)\ dr_2$, is the probability distribution of electron 2 can be though as a charge density. And this density creates the potential energy on the electron 1 because of the electron 2 is

$$V_1^{eff}(r_1) = \int \Psi^*(r_1)\ (1/r_{12})\ \Psi(r_2)\ dr_2 \tag{3}$$

Where the $V_1^{eff}(r_1)$ is called as effective or average potential. And That is a function, depends on r_1 ,since r_{12} is equal to $|r_2-r_1|$ and In the equation(3), the integral is put in r_2.Hence the effective one-electron Hamiltonian operator can be written by

$$\hat{H}_1^{eff}(r_1) = -\frac{1}{2}\nabla_1^2 - \frac{2}{r_1} + V_1^{eff}(r_1) \tag{4}$$

In this equation, the first terms is the kinetic energy of electron, the second term is the potential energy because of the electron- nucleus interaction and the last term is its potential energy by reason of its interaction between other electron. The Schrödinger equation following that operator can be written as

$$\hat{H}_1^{eff}(r_1)\psi(r_1) = \varepsilon_1\psi(r_1) \tag{5}$$

It can be also formed the same equation for, $\psi(r_2)$ However It is not necessary in order to have the same functional form both of them. Only considering one equation like equation (5) is enough for us. That equation is Hartreee-Fock equation for a Helium atom and when it is solved, the best orbital wave function is obtained for a Helium atom.

Though the equation (5) is realized by a physical claim, ıt can be reproduced directly by using the variation princible to the helium atom's energy in an orbital approximation,

$$E = \int\int \psi^*\left(\vec{r}_1\right)\psi^*\left(\vec{r}_2\right)\hat{\mathrm{H}}\psi\left(\vec{r}_1\right)\psi\left(\vec{r}_2\right)d\vec{r}_1 d\vec{r}_2 \tag{6}$$

the ψ is supposed as the normalized at here. By solving this equation, we find

$$\mathrm{E} = \mathrm{I}_1 + \mathrm{I}_2 + \Gamma_{12} \tag{7}$$

Where,

$$\mathrm{I}_i = \int \psi^*\left(\vec{r}_i\right)\left[\frac{-1}{2}\nabla_i^2 - \frac{Z}{r_i}\right]\psi\left(\vec{r}_i\right)d\vec{r}_i \quad i=1, 2, 3,..... \tag{8}$$

And,

$$\Gamma_{12} = \int\int \psi^*\left(\vec{r}_1\right)\psi^*\left(\vec{r}_2\right)\frac{1}{r_{12}}\psi\left(\vec{r}_1\right)\psi\left(\vec{r}_2\right)d r_1 d\vec{r}_2 \tag{9}$$

The Γ_{12} is called a Coulomb integral due to having a classical explication of the interaction between two charge distributions.

Let us examine ε_1 (eigenfunction) as physical meaning, the quantity of ε_1 is known as its orbital energy. Then, the equation (5) is multiplied by $\psi^*(r_1)$ on the left side and integrated

$$\int dr_1 \psi^*(r_1) \hat{H}_1^{eff}(r_1) \psi(r_1) = \varepsilon_1 \tag{10}$$

The finally, By means of equation (4) , (8) and (9)

$$\varepsilon_1 = \mathrm{I}_1 + \Gamma_{12} \tag{11}$$

Hence, total energy of helium atom, is not sum of its orbital energies can be seen on the equation (12)

$$\varepsilon_1 + \varepsilon_2 = (\mathrm{I}_1 + \Gamma_{12}) + (\mathrm{I}_2 + \Gamma_{12}) \neq \mathrm{E} \tag{12}$$

If the equation (11) and (7) is matched,

$$\varepsilon_1 = \mathrm{E} - \mathrm{I}_2 \tag{13}$$

In accordance with equations above, I_2 is the energy of helium ion as well as ε_1 (orbital energy) is an estimation to the ionization energy of helium atom.

$$-\varepsilon_1 \approx \mathrm{IE} \tag{14}$$

The equation (14) is known as Koopmans's approximation. This is an approximation being used not only to calculate the neutral atom energy of the same

orbits but also its ionization energy in Hartree-Fock approximation [21-23].

2.2.1. Antisymmetric Wave Functions

The electronic wave function is physically a request to be antisymmetric due to the fact that the electron is a fermion, so the molecule wave function defines the system must be ψ antisymmetric in accordance with Pauli exclusion princible. A single electron wave function must be indicated for each electron in molecule. In the molecule, each electron is expressed with the wave function of single electron molecular orbital $\Psi(x_i,y_i,z_i)$ being a function respects to x_i, y_i and z_i coordinates. The wave function Ψ of whole system is formed at the simplest method as product of single electron molecular orbital wave functions each other by means of Hartree product [24].

$$\Psi\left(\vec{r}\right) = \psi_1\left(\vec{r}_1\right)\psi_2\left(\vec{r}_2\right)\cdots\psi_n\left(\vec{r}_n\right) \tag{15}$$

The wave function is obtained via Hartree product is not enough because the sign of the wave function don't change when two electrons alter their orbitals. So that, an antisymmetric wave function must be had in order to realize the exchanging of electrons. The Slater determinant is composed by using the combination of molecular orbitals is the simplest antisymmetric wave function because of abundance of electrons instead of two electrons [25].

$$\Psi(1,2,...,N)=\frac{1}{\sqrt{N!}}\begin{vmatrix}\psi_1(1) & \psi_2(1) & ... & \psi_N(1)\\ \psi_1(2) & \psi_2(2) & ... & \psi_N(2)\\ \vdots & \vdots & \vdots & \vdots\\ \psi_1(N) & \psi_2(N) & ... & \psi_N(N)\end{vmatrix} \quad (16)$$

Hence, The Hartree-Fock method can be examined for the complicated atoms but the new term appears at here such as electron spin being neglected until now. This situation explains that the different-spin (up 1/2 or down -1/2) two electrons occupy the 'closed-shell' molecular orbital instead of one electron in each molecular orbital. α function is for the spin-up(1/2)electron and β function is for the spin-down(-1/2) electron.

A spin orbital is created by product spin function to a molecular orbital wave function as;

$$\psi^{\alpha}(x,r)=\psi(r)\alpha(\uparrow) \text{ and } \psi^{\beta}(x,r)=\psi(r)\beta(\downarrow) \quad (17)$$

Now, Again single electron molecule orbital is generated by using the Linear Combination Method of Atomic orbitals the specific coefficients for each atom [26] like,

$$\psi_i = \Sigma\, C_{ik}\emptyset_k \quad (18)$$

ψ_i: single electron molecular orbital function

C_{ik}: The subscription coefficient of k^{th} atomic orbital wave function to single electron molecular orbital.

$\emptyset_k$: k^{th} atomic orbital wave function

Single electron molecular orbital can be described the best effective by

defining atomic orbital for the molecule. In addition to that, the total electronic wave function is attained by acquiring the single electron spin-orbital molecular wave function with spin status of electrons the aim of LCAO. That can be again formulated with Slater Determinant.

$$\Psi(1,2,...,2N)=\frac{1}{\sqrt{2N!}}\begin{vmatrix} \psi_1\alpha(1) & \psi_1\beta(1) & ... & \psi_N\alpha(1) & \psi_N\beta(1) \\ \psi_2\alpha(2) & \psi_2\beta(2) & ... & \psi_N\alpha(2) & \psi_N\beta(2) \\ \vdots & \vdots & \vdots & \vdots & \vdots \\ \psi_N\alpha(2N) & \psi_N\beta(2N) & ... & \psi_N\alpha(2N) & \psi_N\beta(2N) \end{vmatrix} \quad (19)$$

It is clear that the changing of first row refers to the exchanging of two electrons in the determinant and its sign alters. Also, all spin-orbital wave functions were normalized and so the total electronic wave function of the molecule is obtained close value to the real value by more developing this function in the LCAO method.

2.2.2. Density Functional Theory (DFT)

One of the most successful and widely-used quantum mechanical approaches of the examination the electronic structure of many body systems, in particular atoms, molecules, and the condensed phases is Density Functional Theory (DFT) [27]. Vibrational frequencies, geometric parameters, and binding energy of molecules are calculated by DFT. Moreover, DFT is used to analyze atoms in the focus of strong laser pulses, classical liquids, super conductivity as well as it is studied for other fields, like quantum chemistry, biology and mineralogy, etc.[28-29]. Because of the fact that the results of the calculations based on DFT model agreement with the experimental data are preferable and the cost of computational is

low much, DFT is well-known for calculations in molecular physics as compared with conventional ways, for instance Hartree-Fock Theory and its toutomers. In contrast, some atomic system which has a few atoms may be calculated more correct via Hartree-Fock(HF) Theory [30]. However, DFT method is more suitable for the calculation of a molecule has 10 or anymore atoms since DFT takes into account the electron correlation energy with unlike HF method. Contrary to the logic of HF approximation, DFT method bases on writing Hohenberg and Kohn's electron system as the electronic ground state energy functional depend on the electrons density (ρ) on account of excessive electrons in 1964 [31].Hence, the ground state features can be predefined by comprising the density of ground state and energy functional.

As known, HF method begins an exact Hamiltonian but the wave function is formed as product of a single electron wave functions. On the contrary, DFT method starts a Hamiltonian compatible with the multiple-electrons system by aim of the 'ideal' exact wave function. The solution for that is found the 'ideal' system the closest to the real system by optimizing its situation.

In HF model, the energy is equal to;

$$E^{HF}=E^{electron\text{-}core}+E^{core}+E^{coulomb}+E^{exchange\text{-}correlation} \quad (20)$$

$E^{electon\text{-}core}$: *Energy between electron and nucleus*

E^{core} : *Repulsive energy between cores*

$E^{coulomb}$:*Repulsive energy between electrons*

$E^{exchange\text{-}correlation}$: *Spin correlation energy*

In DFT model, the energy is

$$E^{DFT}=E^{electron\text{-}core}+E^{core}+E^{coulomb}+\mathrm{E}_{XC}[\rho] \tag{21}$$

The last energy term is related to (ρ) the exclusive difference between two models.

Then, the exchange-correlation energy is created as the integral of total electron density function in this method;

$$\mathrm{E}_{xc}=\int \rho\left(\vec{r}\right)\varepsilon_{xc}\left[\rho\left(\vec{r}\right)\right]d\vec{r} \tag{22}$$

$\rho(r)$ is the electron density matrix, ψ_i is composed by the help of Kohn-Sham orbitals and The equation for the system being had N electrons is written like that;

$$\rho\left(\vec{r}\right)=\sum_{i=1}^{N}\left|\psi_i\right|^2 \tag{23}$$

$\varepsilon_{xc}\left[\rho\left(\vec{r}\right)\right]$ term is the exchange-correlation energy for each electron in the stable density of a homogenuous electron gases state. Kohn-Sham wave functions are derived from Kohn-Sham equations such as a system having N electrons,

$$\left\{\frac{-1}{2}\nabla_1^{\,2}-\sum_{i}^{nucleus}\frac{Z_i}{r_{i,1}}+\int\frac{\rho\left(\vec{r}_2\right)}{r_{12}}d\vec{r}_2+V_{xc}\left(r_1\right)\right\}\psi_1\left(\vec{r}_1\right)=\varepsilon_i\psi_i\left(\vec{r}_1\right) \tag{24}$$

ε_i terms the Kohn-Sham orbital energy. The exchange-correlation potential (V_{xc}) is

derivative of the exchange-correlation energy functional,

$$V_{xc}[\rho] = \frac{\delta E_{xc}[\rho]}{\delta \rho} \tag{25}$$

When the E_{xc} is known, V_{xc} can be calculated.

Kohn-Sham equations are found out in the self-consistent-field (SCF). For this reason, Initially A electron density $\rho(r)$ is needed to compute E_{xc}. supposing a commencement to Kohn-Sham orbitals is requested to determine the electron density. This prediction is obtained by a set of basis functions being included the extended basis functions' coefficients. V_{xc} is worked out by E_{xc} depend on the electron density. Kohn-Sham equations are resolved in order to attain a set of improved Kohn-Sham orbitals. The set is used to calculate better electron density. This following procedure is carried on until exchange-correlation energy and the electron density remain slightly toleration unvarying.

2.2.2.1. B3LYP Method

Hartree-Fock (HF) model, based on wave mechanic is not suitable for the exchange-correlation energies due to not including the correlation energies. However, it is convenient for the kinetic energy. On the other hand, Density functional theory (DFT) model is agreement with experimental values because of containing the exchange and correlation energies. So that, the several mixed models was formed for the exact energy instead of both HF and DFT such as BLYP, B3LYP,

being used more commonly than others. The standard local exchange functional with the gradient correction of Becke is associate by BLYP [32], uses the Lee-Yang-Parr correlation functional and It comprises density gradient terms [33]. Then, [34] Becke proposed that Becke3LYP includes a hybrid of exact (Hartree-Fock) exchange with local Exchange both gradient-corrected exchange and correlation terms. Moreover, in 20% HF, 8% Slater and 72% is the Becke-88, B3 indicates how much of the exact exchange is blended. The exchange-correlation functional provided by him was

$$E_{xc}=(1-a_0)\,E_x^{LSDA}+a_0\,E_x^{HF}+a_x\Delta E_x^{B88}+E_c^{LSDA}+a_c\Delta E_c^{PW91} \quad (26)$$

Here ΔE_x^{B88} is gradient correction of Becke to the exchange functional and $ac\Delta E_c^{PW91}$ is the Perdew-Wang gradient correction to the correlation functional [35].Becke recommended a_0=0.2, a_x=0.72 and a_c=0.81parameters based on fitment to heats of constitution of small molecules. The coefficients a_0, a_x and a_c proposed by Becke is used in the Becke3LYP in Gaussian92/DFT however it uses LYP for the correlation functional. The VWN local correlation expression is utilized to maintain the distinct coefficients of local and gradient corrected correlation functional. Because, the LYP does not involve with ease sectional local component.

$$E_{xc}^{B3LYP}=(1-a_0)\,E_x^{LSDA}+a_0\,E_x^{HF}+a_x\Delta E_x^{B88}+a_cE_c^{LYP}+(1-a_c)\,E_c^{VWN} \quad (27)$$

2.2.3. Basis Functions and Basis Sets

In the molecule, the molecular orbital function of each electron is comprised as a result of Linear Combination of atomic orbital functions. The atomic orbitals are

called as basis functions. A group basis functions refer to each atom in the molecule [24, 34].The basis sets are a numerical table computing mathematically to find the probability position of electrons. Also, the “basis set” generally refers to the set of (nonorthogonal) one-particle functions preferred to construct molecular orbitals in quantum chemistry. Two molecular orbitals of the well known and the most common are Slater Type Orbital (STO) and Gaussian Type Orbital (GTO).

2.3.1. Slater Type Orbital (STO)

Slater Type Orbitals being had the spherical symmetry orbitals are generally used in any molecule, has two electrons. That is, the orbitals is formed the obtained functions by solving the schrödinger equation for the hydrogen atom and another single-electron ions.

$$\psi_{\zeta,n,l,m}(r,\vartheta,\varphi) = NY_{l,m}(\vartheta,\varphi)r^{n-1}e^{-\zeta r} \tag{28}$$

N is the normalization constant. The $Y_{l,m}(\vartheta,\varphi)$ is the spherical harmonic for the single-electron like hydrogen. The ζ term indicates a constant for the given atomic orbital type (s, p, d, f ,...) and n, l, m are the quantum numbers. Slater Type Orbitals are very successful to describe atomic orbitals having an electron distribution in the spherical symmetry but are not enough to generate molecular orbitals having an electron distribution in the axial symmetry. The Gaussian Type Orbitals are preferred instead of that so as to eliminate deficiencies.

2.2.3.2. Gaussian Type Orbital (GTO)

The Gaussian Type Orbitals chosen in the Ab-Initio calculation method are

used to create the molecular orbitals including an electron distribution in the axial symmetry. The Gaussian Type Orbitals are derived from primitive gaussian functions denoted by

$$g_{i,j,k}(r_i - r_p) = (x_1 - x_p)^i .(y_1 - y_p)^j .(z_1 - z_p)^k e^{-\gamma(r_1 - r_p)^2} \quad (29)$$

i, j and k are positive integer. x_p, y_p and z_p are the center of coordinate system and x_1, y_1 and z_1 are the cartesian coordinates of the electron. The primitive gaussian functions are called according to the number of i, j, and k. When the sum of i, j, and k integers is equal to zero, one and two, the gaussian functions are called as s-type, p-type and d-type Gaussian, respectively. s, p, d and f terms mean the primitive gaussian functions used to describe atomic orbitals and they have the relevant symmetrical property. The Gaussian functions are the linear combination of the primitive gaussian functions. The basis function made up from a single primitive gaussian function is named as the uncompressed basis function and the compressed basis function for the included more primitive gaussian functions. The written a formula down for a compressed basis function,

$$S_i = \sum_t b_{it} g_t \quad (30)$$

S_i : the linear combination of the gaussian functions.

g_t : any primitive gaussian function in the given set.

b_{it} : constant coefficients for the set

The atomic orbitals can be formed by using this formula down,

$$\psi_j = \sum_i C_{ji} S_i \tag{31}$$

The Gaussian basis sets are varied due to the defining of ‘closed shell’ and ‘open shell’ orbitals. There are two type standard Gaussian basis sets to characterize ‘open shell’ orbitals alter with respect to the number of primitive gaussian basis functions[36].

a. Double-zeta (ζ) basis sets (v-hnG)

The zeta (ζ) function controls the width of orbitals. The closed shell atomic orbitals obtained by double-zeta basis sets are expressed a compressed gaussian function being contained a number of m primitive gaussian functions. The v, h, and n are integer numbers and G defines the Gaussian. The’ open shell’ orbitals have two compressed Gaussian functions including a number of h and n primitive Gaussian functions. For instance 3-21G, 4-31G and 6-31G basis sets for the double zeta basis sets. The well-definition of atomic orbitals depends on the number of primitive Gaussian functions in the basis sets.

b. Triple-zeta (ζ) basis sets (v-hn1G)

As the comparisons with the double-zeta basis sets, the closed shell atomic orbitals got by triple-zeta basis sets are shown a compressed gaussian function being enclosed a number of m primitive gaussian functions. The v, h, and n are integer numbers and G defines the Gaussian. The’ open shell’ orbitals have three compressed Gaussian functions including h, n primitive Gaussian functions and 1

primitive Gaussian function. For instance, 6-311G and 6-321G basis sets for the triple-zeta basis sets.

c. Diffuse Functions

The diffuse functions are preferred to describe better electrons which are relatively far from the nucleus because the zeta basis sets are not enough so as to attain well the atomic orbitals. Furthermore, these functions provide more accurate determination of anions or neutral molecules with unshared pairs and the understanding preferable weak (van der Walls) bonds intermolecules. The presence of diffuse functions is indicated by adding a plus (+) sign to the basis set designator: for example, 6-31+G. (As these are s and p orbitals, the symbol is shown front of the G.) Second plus (+) sign point out diffuse functions inserted for hydrogen atoms[37].

d. Polarization Functions

Thereto developement of basis functions is obtained by the addition of d-orbitals to all heavy (non-hydrogen) atoms. These are not preferred in bond formation having the d-orbitals of transition metals for some organic compounds. They are useful to allow how shift the center of an orbital away is from the position of the nucleus. For instance, a p-orbital on carbon is polarized away from the nucleus owing to mixing into it a d-orbital which is lower symmetry. Moreover, compounds which involve second-row elements are more exactly designated by the presence of polarization. The polarization functions are symbolized by star sign (*) in the Pople notation. This first star implies the addition of d-orbital to p-orbital for second-row elements (6-31G*).Second star (**) indicates the addition p-orbitals to only hydrogen s-orbital to provide the describing better of the orbitals. So that, the basis sets which

have second star (**) are relevant for the systems which hydrogen bonding occurs[38

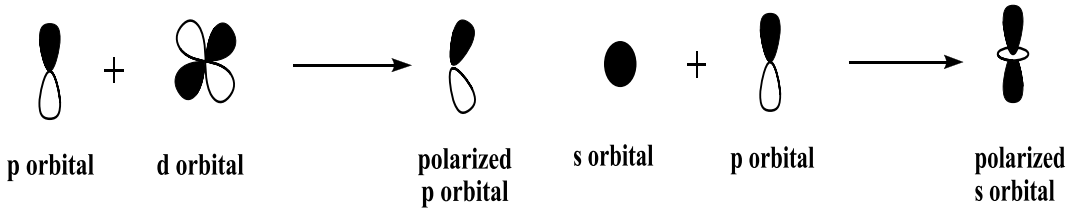

Figure 1. The polarizaiton of s and p orbitals

CHAPTER 3

3.1. The Sorts of Spectroscopy

Initially, the spectrum is a measured graph of light intensity versus some property of light like wavelength or wave number. The spectrometer is a instrument used to measure a spectrum. The spectroscopy is the investigation of interaction between light and matter. There are several spectroscopes in order to investigate some properties of especially organic molecules such as infrared (IR), Raman, nuclear magnetic resonance (NMR), ultraviolet spectroscopy(UV).

3.1.1. Infrared Spectroscopy

The infrared spectroscopy examines how the electromagnetic wave interacts with a matter in infrared region. When the electromagnetic wave is sent on a sample, the light is either absorbed or emitted by the matter.[39] The IR spectroscopy is conducted so as to determination of functional groups (specific chemical bonds) of the molecules had different characteristic absorption frequencies. The wave number being number of waves in per unit length is used in the plot spectrum because the wave number is directly proportional to IR absorption energy and frequency. The measurements are usually obtained in mid- infrared region whose wavelength is approximately 2.5-50μm and wave number is fundamentally between 4000 and 400 cm^{-1}. As most organic molecules have vibrational energy with the range of this region, IR spectroscopy supplies several advantages and opportunity in order to identify molecule IR spectroscopy is approvable universal in terms of that many

types of matters involving solids, liquids, gases, semi-solids have a infrared spectrum. The absorptions bands and band intensities also indicate the concentrations and functional group bonded chemically to molecules. Moreover, the information about pH and hydrogen bonds characteristic of molecule mainly could be obtained from band widths [40]. An infrared spectrum of any molecule is reached easily in roughly five minutes or less.

All measurements obtained based on two main theorems such as classical and quantum mechanical.

3.1.1.1. Classical Theorem

In accordance with the classical theorem, altering electrical dipole moment having three components (μ_x, μ_y, μ_z) in Cartesian coordinate is necessary to attain the vibration value of a molecule during the molecule vibrations. When absorbed the light being frequency (ν), the electrical dipole moment of the molecule changes in a direction or others so this vibration is observed in IR region. in relation to simple harmonic approximation, the electrical dipole moment can be written as a function of **φ** normal vibration coordinate for the small amplitudes by neglecting second order term and the latter in Taylor series like the equation (32) down;

$$\vec{\mu} = \vec{\mu}_0 + \sum \left\{ \frac{\partial \vec{\mu}}{\partial \varphi_m} \right\}_0 \varphi_m \tag{32}$$

The electrical dipole moment or its any components must change to be the vibration active in keeping with the classical theory like the equation (33).[41]

$$\left(\frac{\partial \vec{\mu}_i}{\partial \varphi_m}\right) \neq 0 \quad (i = x, y, z) \tag{33}$$

3.1.1.2. Quantum Mechanical Theory

The electrical dipole moment or its any components must be different from zero to be the transition between Ψ_g and Ψ_e are a wave function of ground and excited state vibration energy, respectively consistent with quantum mechanical theorem.

$$\mu_{ge} = \int_{-\infty}^{\infty} \Psi_g \mu \Psi_e dr \neq 0 \tag{34}$$

r represents normal coordinate and $\boldsymbol{\mu}$ indicates electrical dipole moment operator. Then, articulated by a displacement of atoms during the vibration, *r* has a small value. Hence, the $\boldsymbol{r}^2$ can be omitted and the following terms in the equation above. Substituting the terms up to *r* of Eq.(32) in Eq. (34).

$$\mu_{ge} = \mu_0 \int_{-\infty}^{\infty} \Psi_g \Psi_e dr + \sum \left\{ \left(\frac{\partial \vec{\mu}}{\partial \varphi_m}\right)_0 \int_{-\infty}^{\infty} \Psi_g \varphi_m \Psi_e dr \right\} \tag{35}$$

is obtained the equation (35).

When Ψ_g and Ψ_e are orthogonal ($g \neq e$) to each other, the first term will be zero.

$|\boldsymbol{\mu}_{ge}|^2$: is proportional to the transition probability between two Vibrational energy states.

Finally, the equation (36) is formed by using the equation (35) under this condition.

$$\mu_{ge} = \sum \left\{ \left(\frac{\partial \vec{\mu}}{\partial \varphi_m} \right)_0 \int_{-\infty}^{\infty} \Psi_g \varphi_m \Psi_e \, dr \right\} \tag{36}$$

And the changing dipole moment during the vibration of molecule to be infrared active in IR spectroscopy is approved by,

$$\left(\frac{\partial \vec{\mu}}{\partial \varphi_m} \right) \neq 0 \tag{37}$$

3.1.2. Raman Spectroscopy

When the light interacts with the sample, the light is absorbed, scattered. The Raman spectroscopy is rooted in the measurement of the scattered light by directing the powerful laser being created Visible or Near-Infrared monochromatic radiation to the sample at certain angle (often 90°).The spread of light being the energy of the incident photon and the scattered photon are same is elastic (Rayleigh scatter).However, the Raman scattering is inelastic due to changing the energy of incident light. Whereas Rayleigh scattering does not give any information about the vibration transitions, the altering energy of the incident photon and the scattered photon is the difference between the Vibrational energy levels of the molecule. Therefore the Raman spectroscopy is used in order to examine the Vibrational energy levels of the molecule and analyze the quantitative value and generally the qualitative value of organic, inorganic and biological molecules.

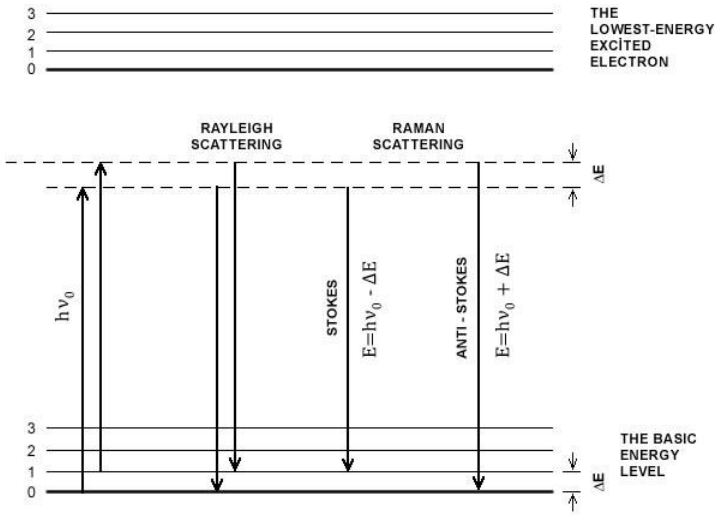

Figure 2: Stoke and anti-stoke scattering

The molecules place at the different vibrational energy levels after the molecules' interaction with photon such as stokes scattering and anti-stokes scattering having negative and positive value, respectively. While the molecule vibrates, the temporary and periodic dipole moment (polarisable) appears to create the Raman scattering because of the electric field of incident light inside the molecule. The intensity of Raman is equal to square the changing polarisable speed during interaction of molecule with the light.

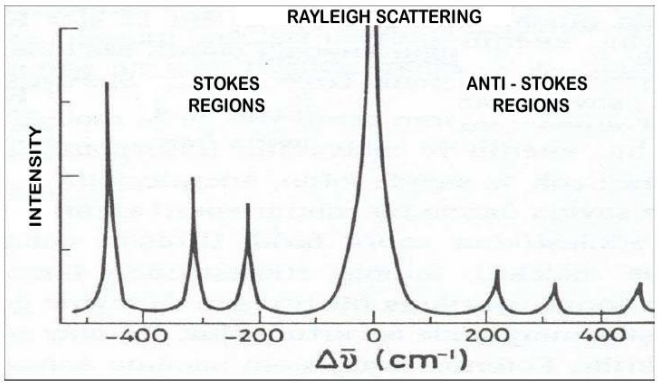

Figure 3: Raman scattering and Rayleigh scattering graph

In the last, there are several advantages of Raman spectroscopy in comparison with Infrared spectroscopy. The low-vibration compounds (-S-S-, –C-O-C-, narrowing ring and extending ring) which can not be studied via Infrared spectroscopy but they can be investigated easy with the aim of Raman spectroscopy. Moreover, all solvents used for IR spectroscopy and very low-vibration water in addition to the solvents are utilized for Raman spectroscopy with their request Raman shifts. The superiority of Raman spectroscopy scan whole region of IR (near, middle, far) spectrum[42].

3.1.3. Nuclear Magnetic Resonance Spectroscopy (NMR)

The working princible bases on the measurement of the excited rotation energy level of the nuclei absorbing electromagnetic radiation in the range of radio wave 4-900 MHz(75m-0.33m).The basic properties of nuclei or proton are to have own mass, charge and spin angular momentum. Magnetic dipole moment (***μ***) due to spin angular momentum is formulated;

$$\mu = \rho\left(\frac{e}{2m_p}\right)\hbar\sqrt{\imath(\imath+1)} \tag{38}$$

m is proton mass, ***ρ*** and ***ħ*** are constants.

$\left(\frac{e}{2m_p}\right)$ ⟶ is named as the nucleus magnetron

$\hbar\sqrt{\imath(\imath+1)}$ ⟶ is called as the magnitude of spin angular momentum.

$\left(\frac{\mu}{\hbar\sqrt{\imath(\imath+1)}}\right)$ ⟶ is known as gyro-magnetic ratio(γ).

When exposed to the magnetic field (*H*), magnetic moment of nuclei moves circular surrounding magnetic field. If gyro magnetic ratio (γ) and magnetic field (*H*) are known, the written formula down is obtained to calculate the magnetic moment by starting the torque formula;

$$\frac{d\vec{\mu}}{dt} = \gamma \vec{\mu} \times \vec{H} \tag{39}$$

Especially, Once the magnetic field is applied through z-direction ($H_x=0$, $H_y=0$ *and* $H_z= H_0$).

$$\frac{d\vec{\mu}_x}{dt} = \gamma \vec{\mu}_y \times \vec{H}_0 \tag{40}$$

$$\frac{d\vec{\mu}_y}{dt} = \gamma \vec{\mu}_x \times \vec{H}_0 \tag{41}$$

$$\frac{d\vec{\mu}_z}{dt} = 0 \tag{42}$$

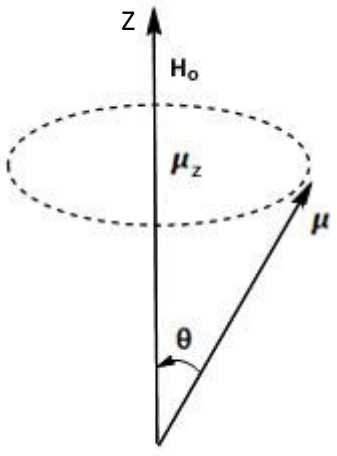

Figure 4. Precession motion

Interaction energy between magnetic field (H) and the magnetic moment ($\boldsymbol{\mu}$) is,

$$E = -\vec{\mu}.\vec{H} = \mu H \cos\theta \tag{43}$$

In accordance with quantum mechanic, ıt is supposed that angular momentum is quantized in space. So, the angle (ɵ) has special values. For instance, the angle(ɵ) has only two values for spin (1/2) of proton and the spin angular momentum is only equal to (1/2)$\boldsymbol{\hbar}$ or (-1/2)$\boldsymbol{\hbar}$**.** The magnetic quantum numbers are (1/2) and (-1/2) at here. If spin and magnetic field are at same direction or opposite direction, the energy value is negative or positive, respectively. When the nucleus absorbs energy being equal to difference between two states with proper frequency, this is called nuclear magnetic resonance. On the other hand, chemical shift is based on the measurement of an electric field comprised in molecule with effect of external magnetic field and internal (induction) magnetic field occurred in nucleus because of this electric field. The internal magnetic field and the external magnetic field are opposite direction to each other. The net magnetic field of the nucleus exposed to the external magnetic field is:

$$H = H_e - H_i = H_e(1-\lambda) \tag{45}$$

The λ depending on only electron order surrounding the nucleus is dimensionless correlation constant and its value is 10^{-5} for proton [41]. The chemical shift being its reference tetra methyl slain (TMS) is formulized in frequencies (f) by

$$f_{kl} = (f_k - f_l) \text{x} 10^6 / f_e \quad ppm \tag{46}$$

The NMR spectroscopy is used to research the structure of covalent compounds, identifying of organic compounds. The types of NMR spectroscopy are ^{1}H, ^{11}B, ^{13}C, ^{19}F, ^{15}N and ^{31}P having spin quantum number (1/2). The most useful NMR spectroscopes are ^{13}C and ^{1}H-NMR since they provide more defining and detailed information.^{1}H-NMR investigates information of a number of protons, aromatic groups, methyl groups attached to a CH_2 and CH_3 groups adjacent to methyl group. Furthermore, ^{13}C-NMR reveals information about a number of carbons, four different carbon atoms on an aromatic ring and carbonyl carbon [43].

3.1.4. UV/Visible Spectroscopy

Molecular absorption spectroscopy bases on the measurement of the absorbed energy of a light having 160-780 nm ($3x10^{14}$-$3x10^{16}$) by valence electrons. This spectroscopy is made use of the analysis functional groups and their quantity properties for many organic and inorganic molecules. Moreover, the transitions among **σ, π** and **n** orbitals for organic molecules, the transition between **d** and **f** orbitals for the coordination complexes and the charge transfers for both organic and complex molecules are investigated with the aim of Ultraviolet/Visible absorption spectroscopy. In the organic molecules, the electrons providing the absorption are the bonding electrons of **σ** and **π** bonds and the electrons(unpaired) of **n** nonbonding orbitals like oxygen , sulphur, nitrogen and halogens. The sigma orbitals are generally come about between s-s, p-p or s-p orbital in the organic molecules. The Pi orbitals are formed by attaching two p orbitals side by side. There are four types electronic transitions such as $\sigma \rightarrow \sigma^*$, $n \rightarrow \sigma^*$, $\pi \rightarrow \pi^*$ and $n \rightarrow \pi^*$ in the fig. 5,

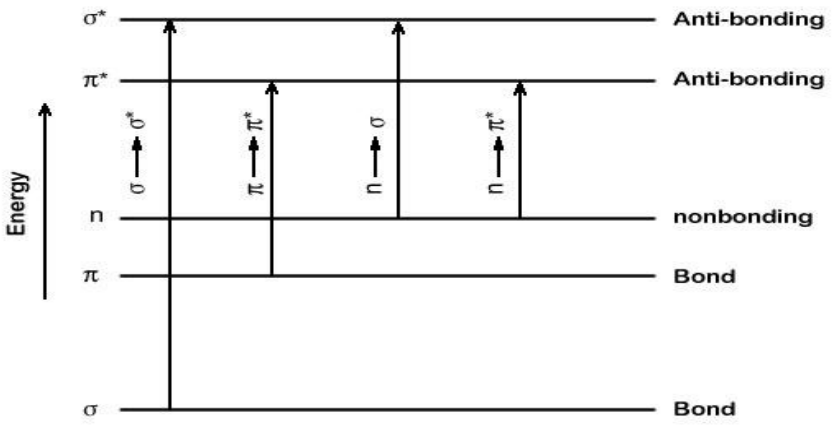

Figure 5: Electronic transitions for a organic molecule

When the **σ** bond's electron absorbs the light placing in the UV region, the electron is excited to anti-bonding (**σ***).Hence, the **σ→ σ*** transition requesting high energy as compared to other transition occurs. For example, the CH_4 molecule consisting of only C-H bonds. This molecule has only a **σ→ σ*** transition and has a maximum absorption 124 nm. Furthermore the **n→ σ*** transition which has absorption peak in the range of 150-250 nm(less energy than the **σ→ σ*** transition) is seen in the compounds containing unpaired electrons. The **n→ σ*** transition peak shifts to lower wavelength in the polar solvents such as water and ethanol and the number of organic functional groups including a **n→ σ*** transition is very few. And than, the **π→ π*** and **n→ π*** transitions appear by absorbing a light being in the range of 200-700 nm are the most common transitions. These transitions occur in the organic molecules involving the unsaturated functional group because of having the **π*** orbitals. Also, the characteristic difference between these transitions is the effect of the solvent on the wavelength of peaks. That is, when the polarity of the solvent increases for the **n→ π*** transitions, the wavelength shifts into lower wavelength (blue region) but this shift is generally to higher wave length (red region) for the **π→**

π^* transitions. Moreover, almost all transition metals absorb the UV/Visible source due to the transition energy between various energy levels of 3d and 4d orbitals and the electronic transition of 4f and 5f electrons for the Lanthanide and actinide series which have narrower spectrum in comparison with organic and inorganic spectrum. The Lanthanide and actinide series are not thrilled from the solvents and the surrounded electrons because of the narrow bands. Besides, one of the components of complex compound is a donor electron and other is an acceptor electron to have the charge transition absorption [44].

3.2. Skeletal and Group Vibrations

All atoms placing in molecule move continuously between them above the absolute temperature. Each atom has three independence degrees (x, y, z) in 3D cartesian coordinate. That is, when the molecule has N atoms, it has 3N independence degree. However, that independence degree is 3N-6 for the nonlinear molecules and 3N-5 for the linear molecules. The 6 and 5 numbers represent us the total of transition and rotation modes. Group frequency is known as each group vibrates with different frequency in the molecule. That informs us about atom groups in molecule. For instance, the absorption of C-H bond is a symmetric stretching between 2850 and 2900 cm^{-1} or antisymmetric stretching between 2940 and 2980 cm^{-1} in CH_3 compound. Skeletal vibrations being generally between 1400-700 cm^{-1} originate due to the linear or chain structures in molecule and provide information about molecule structure[45].

3.2.1. The vibration varieties for multiple-atoms molecules

3.2.1.1. Stretching (ν)

Stretching means that one more bonds make tension or compression movement as periodic at same time. Antisymmetric stretching (ν_{as}) and symmetric stretching (ν_s) is their tension and compression movement in opposite direction and at the same direction, respectively

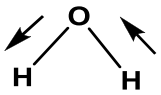

antisymmetric strecthing

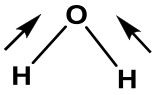

symmetric strecthing

Figure 6. Types of stretching motion

3.2.1.2. Bending (δ)

Bending is divided into four sections such as rocking, scissoring, wagging and twisting means that the angle changes periodical between two bonds. The displacement vector is perpendicular to bonding direction.

3.2.1.2.1. Rocking (ζ)

Rocking being a special type of bending is to alter in angle between two bonds without the changing bond length at the same direction in plane.

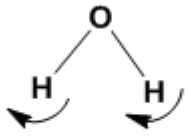

rocking

Figure 7. Rocking motion

3.2.1.2.2. Scissoring (ρ_r)

Scissoring which is another type of bending is to change continuously in angle between two bonds in opposite direction in plane.

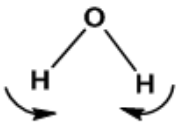

scissoring

Figure 8. Scissoring Motion

3.2.1.2.3. Wagging (ω)

Wagging means that the angle between the bond and the plane changes periodical towards the out of plane at the same direction.

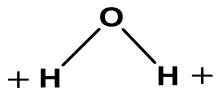

wagging

Figure 9. Wagging motion

3.2.1.2.4. Twisting (K)

Twisting is to alter incessantly in angle between the bond and the plane towards the out of plane in the opposite direction.

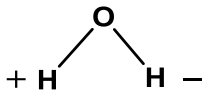

twisting

Figure 10. Twisting motion

3.2.1.3. Torsion

Torsion means that the angle between two planes or the dihedral angle defined by three bond vectors alters.

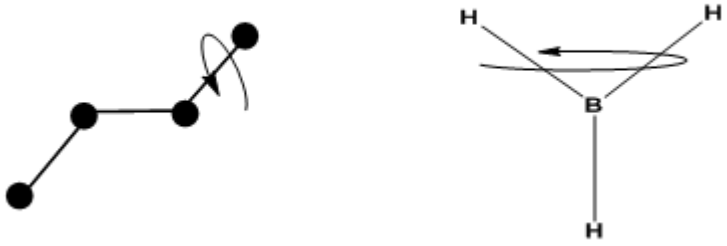

Figure 11. Torsion motions

CHAPTER 4

4.1. Experimental and Computational Details

This multidisciplinary study is composed of two main performances for the characterization of the BPOCPA monomer: (I) experimental measurements and (II) theoretical calculation.

Fort the first performance, the p-benzophenoneoxycarbonylphenyl acrylate is synthesized as reported previously [46]. Namely, 25.0 g, (0.126 mol) HBP and triethylamine 12 mL (7.5 g, 0.126 mol) are dissolved in 150 mL of ethyl methyl ketone (EMK), and the reaction solution is cooled to 0-5°C in ice bath. Then, 26.5 g, (0.126 mol) ABC dissolved in the EMK of 150 mL is added dropwise with stirring at the same temperature for 1 h and 5 h at room temperature, respectively. The solid quaternary ammonium salt obtained is filtered off and washed with access amount of EMK. The organic solution is also washed successively with 5% aqueous NaOH solution, diluted HCl and distilled water, respectively. The product was precipitated by further addition of distilled water, and then collected with the aid of a filter. The solid product is recrystallized repeatedly from ethanol and ethyl acetate. The purification is carried out by column chromatography. Here, the dichloromethane is used as a mobile phase while the silica gel is preferred as a stationary phase[47]. The yield of BPOCPA monomer is observed to be approximately 16 wt%.

Alternatively, the new synthesis method for the monomer is accomplished refluxing ABC and HBP in xylene. 25.0 g (0.126 mol) HBP and 26.5 g, (0.126 mol) ABC are refluxed in xylene of 250 mL for about 3-4 days to produce the dark brown-black impurity in the reaction medium. The suspension is settled down by adding a

small amount of hexane. The monomer, BPOCPA is precipitated from the reaction solution, and then recrystallized from ethanol and ethyl acetate mixture. Surprisingly, the yield of the monomer is found to be about 57 wt%.

For the experimental characterization, the title compound, BPOCPA, is identified by means of ultra violet-visible (UV–vis) spectrometer, Fourier transform infrared (FTIR) spectrophotometer and nuclear magnetic resonance proton chemical shifts (^{1}H NMR). The UV-vis spectra of the products are recorded by the unpolarized light at normal incidence in the wavelength range of 400–700 nm, with a JASCO 430 UV–VIS spectrophotometer. Furthermore, the FT-IR spectra are recorded on a Shimadzu 8400S FT-IR spectrophotometer in the region 400–4000 cm^{-1} with a resolution of 4 cm-1 in the transmission mode. Besides, the NMR spectra being performed with the aid of a Bruker-Spectrospin Avance DPX 400 Ultra-shield ^{1}H-NMR spectrometer in DMSO solution with a frequency of 400 MHz are reported as parts per million (ppm) from the internal standard tetramethylsilane (TMS).

As for the second performance; the optimized molecular structures, UV-vis spectra, thermodynamic properties, vibrational frequencies, atomic charges, NMR spectra, the optical and electrochemical properties such as frontier orbitals (HOMO and LUMO), optical band gap (HOMO–LUMO), electrostatic potential (ESP) with 2D total charge density contour and molecular electrostatic potential (MEP) of the BPOCPA are performed using 2009W version of the GAUSSIAN suite program [48] with molecular visualization program [49] on the personal computer by means of the Becke's three parameter hybrid exchange functional [50] combined with the Lee-Yang-Parr non-local correlation function [51] supplemented with the standard 6-311++G(d,p) [52,53] level of calculation for the first time. Furthermore, the Cartesian representation of the theoretical force constants is computed at the

optimized geometry under C_1 point group. According to the SQM procedure [54, 55], scaling of the force field is carried out using selective scaling in the natural internal coordinate representation [56-57]. Transformation of the force field and subsequent normal coordinate analysis including the least square refinement of the scaling factors, calculations of the potential energy distribution (PED) and the prediction of IR and Raman intensities are examined by VEDA–4 program [58]. Besides, the Raman activities (S_i) calculated by Gaussian 09 program are converted to relative Raman intensities (I_i) using the following relation from the basic theory Raman scattering [59, 60]

$$I_i = \frac{f(\nu_0 - \nu_i)^4 S_i}{\nu_i\left[1 - \exp(-hc\nu_i / KT)\right]} \tag{47}$$

where *h, c, k* are the universal constants and *f* is suitably chosen common normalization factor for all the intensities when ν_0 (cm^{-1}) is the exciting frequency and ν_i is the vibrational wave number of the normal mode. The spectra results are found to be more regular than the experimental ones due to the fact that several vibrations presenting in condensed phase lead to the strong perturbation of infrared intensities of other modes.

The electronic properties of the molecules are also calculated from the total energies (*TE*) and the Koopmans' theorem (*KE*). The ionization potential is determined from the energy difference between the energy of the compound derived from electron-transfer (radical cation) and the respective neutral compound; $IP_{TE} = E_{cation} - E_n$; $IP_{KE} = -E_{HOMO}$ while the electron affinity is computed from the energy difference between the neutral molecule and the anion molecule: $EA_{TE} = E_n - E_{anion}$;

$EA_{KE} = -E_{LUMO}$, respectively. The other important quantities such as electronegativity (χ), hardness (η), softness (ζ), and electrophilicity index (ψ) are deduced from ionization potential and electron affinity values [61-63].

$$\text{Electronegativity } (\chi) : \mu \approx -\chi = -\frac{IP + EA}{2} \tag{48}$$

$$\text{Chemical Hardness } (\eta) \approx \frac{IP - EA}{2} \tag{49}$$

$$\text{Softness } (\zeta) = \frac{1}{2\eta} \tag{50}$$

$$\text{Electrophilicity Index } (\psi) = \frac{\mu^2}{2\eta} \tag{51}$$

4.2. Result and Discussion

In order to identify the BPOCPA monomer, both the experimental and theoretical studies are performed. For the experimental studies, UV–vis, FTIR spectrophotometer and ^{1}H NMR chemical shifts are experimentally investigated for the characterization of the title compound. As for the theoretical examinations, molecular geometry, vibrational frequencies including Infrared intensities and Raman activities, corresponding vibrational spectra, atomic charges, thermodynamic properties, (total energy, heat capacity, thermal energy, entropy and zero-point vibrational energy), dipole moment, softness, electronegativity, chemical hardness, electrophilicity index, ^{1}H and ^{13}C NMR chemical shifts, frontier orbitals (HOMO and LUMO), molecular electrostatic potential (MEP) and electrostatic potential (ESP) with 2D total charge density contour are analyzed for the identification of the

molecule.

4.2.1. Vibrational Symmetry

All molecules studied are composed of 44 atoms and belong to the point group C_1 including only identity (E) operation symmetry element. As well known, N-atomic molecules provide 3N internal modes [64,65] because of the three Cartesian displacements. 6-Mode of them is for translation and rotational modes. Therefore, 126 (3N–6) vibrational modes are described in the title compound.

4.2.2. Conformational Analysis and Molecular Geometry

In order to investigate all possible conformations and the most stable state of the title compound, the detailed potential energy surface (PES) scans in the dihedral angles of C_{17}–C_{16}–C_{30}–C_{24} and C_4–C_{11}–C_{19}–C_{13} are performed by means of B3LYP/6-311++G(d,p) level of theory. As well known, the working principle of the PES scan is based on the minimization of the potential energy with the change of the dihedral angle in all geometrical parameter. In this thesis, the PES scan is performed with the rotation of the dihedral angles changing from 10° to 360° around the bond. The shape of the potential energy as a function of the dihedral angles is given in Fig. 12. The global minimum energies of the most optimized compound are predicted to be about -1262.51660272 au and -1254.36894445 au at B3LYP/6-311G++(d,p) and HF/6-311G++(d,p) levels of calculation, respectively.

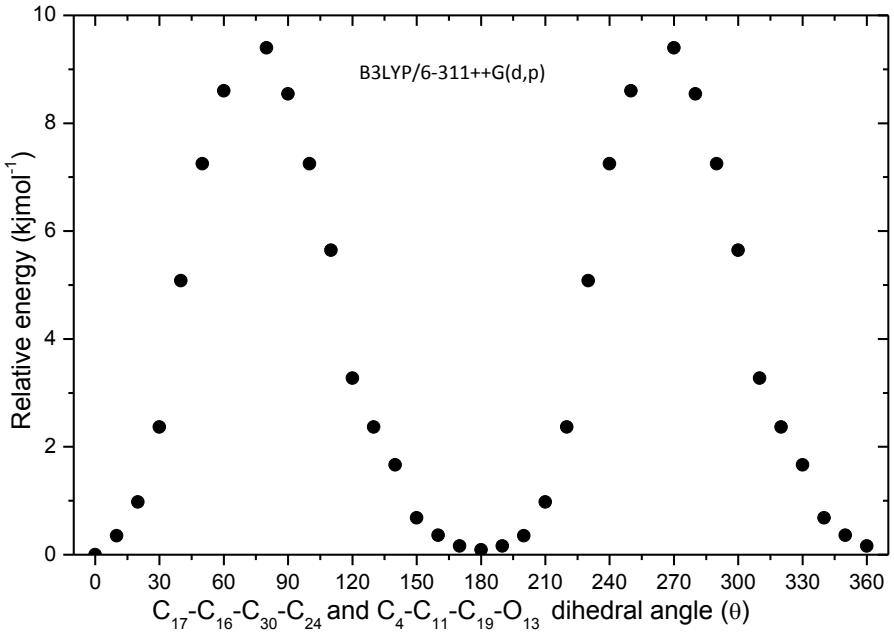

Figure 12. Relative potential energy surface scan for dihedral angles C_{17}–C_{16}– C_{30}–C_{24} and C_4–C_{11}–C_{19}–C_{13} of the BPOCPA.

The (most optimized) molecular structure of the title compound with numbering schema for the atoms is given in Fig. 13. The selected geometric properties such as bond lengths and bond angles of the structure studied in this work are depicted in Table 1. It is clear from the table that all the calculated data are found to be in good agreement with each other and in fact the correlation coefficients are determined to be 0.9973 for bond lengths and 0.9818 for the bond angles. The calculations of HF/6-311++G(d,p) basis set are generally found to be smaller than B3LYP /6-311++G(d,p) ones. Besides, the largest differences of the geometries calculated are noted to be about 0.09 Å (H_{10}-O_{39} and O_{12}-H_{23}) for the bond lengths; 1.22° (C_4-C_{11}-O_{13}) for the bond angles, respectively. This may be attributed to the fact that the phenyl rings appear to be a little distorted from their regular hexagonal symmetry due to the variation of bond lengths and bond angles in these rings for the title compound studied in this work. Thus, the irregular hexagonal symmetry of the

phenyl rings results from the change of the bond angle values at the substitution position (Table 1). As well known, the changes in the bond length or frequency and breakdown of regular hexagonal symmetry of the phenyl ring bring about the changes in charge distribution on the carbon atoms [66,67], being favored by the results of the atomic charge analyses.

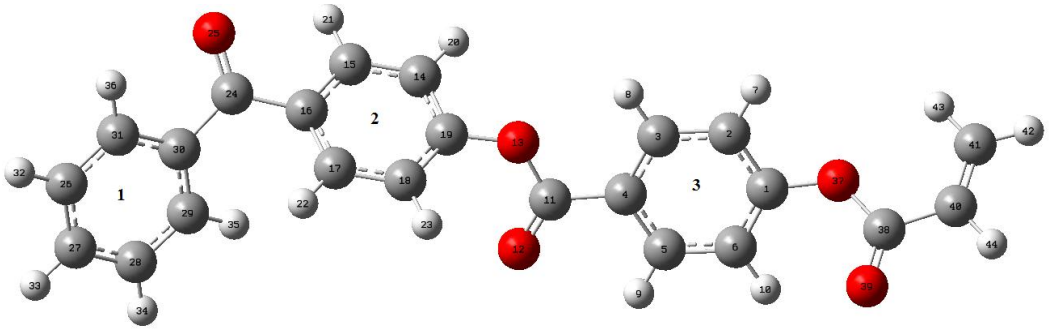

Figure 13. The molecular structure belonging to the BPOCPA monomer

Table 1. Theoretical optimized geometric parameters obtained from B3LYP/6-311++G(d,p) and HF/6-311++G(d,p) levels of theory for the title compound

BPOCPA	**Bond Length(Å)(DFT)**	**Bond Length(Å)(HF)**
C_1-C_2	1.39	1.38
C_1-C_6	1.39	1.38
C_1-O_{37}	1.39	1.39
C_2-C_3	1.39	1.38
C_2-H_7	1.08	1.07
C_3-C_4	1.40	1.39
C_3-H_8	1.08	1.07
C_4-C_5	1.40	1.39
C_4-C_{11}	1.49	1.47
C_5-C_6	1.39	1.38
C_5-H_9	1.08	1.07
C_6-H_{10}	1.08	1.07
H_{10}-O_{39}	2.68	2.58
C_{11}-O_{12}	1.20	1.21
C_{11}-O_{13}	1.37	1.36
O_{12}-H_{23}	2.69	2.79
O_{13}-C_{19}	1.39	1.40
C_{14}-C_{15}	1.39	1.38
C_{14}-C_{19}	1.39	1.38
C_{14}-H_{20}	1.08	1.07
C_{15}-C_{16}	1.40	1.39
C_{15}-H_{21}	1.08	1.07
C_{16}-C_{17}	1.40	1.39
C_{16}-C_{24}	1.50	1.49
C_{17}-C_{18}	1.39	1.39
C_{17}-H_{22}	1.08	1.07
C_{18}-C_{19}	1.39	1.38
C_{18}-H_{23}	1.08	1.07
C_{24}-O_{25}	1.22	1.23
C_{24}-C_{30}	1.50	1.49
C_{26}-C_{27}	1.40	1.39
C_{26}-C_{31}	1.39	1.38
C_{26}-H_{32}	1.08	1.07
C_{27}-C_{28}	1.39	1.39
C_{27}-H_{33}	1.08	1.07
C_{28}-C_{29}	1.39	1.39
C_{28}-H_{34}	1.08	1.07
C_{29}-C_{30}	1.40	1.39
C_{29}-H_{35}	1.08	1.07
C_{30}-C_{31}	1.40	1.39
C_{31}-H_{36}	1.08	1.07
O_{37}-C_{38}	1.37	1.36
C_{38}-O_{39}	1.20	1.21
C_{38}-C_{40}	1.48	1.47
C_{40}-C_{41}	1.33	1.32
C_{40}-H_{44}	1.08	1.07
C_{41}-H_{42}	1.08	1.07
C_{41}-H_{43}	1.08	1.07

Table 1. Theoretical optimized geometric parameters obtained from B3LYP/6-311++G(d,p) and HF/6-311++G(d,p) levels of theory for the title compound (continued)

Bond Angles(°)		
C_2-C_1-C_6	121.28	121.65
C_2-C_1-O_{37}	116.56	115.83
C_6-C_1-O_{37}	122.04	122.44
C_1-C_2-C_3	119.51	119.39
C_1-C_2-H_7	119.29	119.23
C_3-C_2-H_7	121.20	121.38
C_2-C_3-C_4	120.08	119.92
C_2-C_3-H_8	120.07	120.24
C_4-C_3-H_8	119.85	119.84
C_3-C_4-C_5	119.52	119.77
C_3-C_4-C_{11}	122.69	122.02
C_5-C_4-C_{11}	117.79	118.22
C_4-C_5-C_6	120.73	120.67
C_4-C_5-H_9	118.86	119.15
C_6-C_5-H_9	120.41	120.18
C_1-C_6-C_5	118.88	118.60
C_1-C_6-H_{10}	120.42	120.68
C_5-C_6-H_{10}	120.70	120.72
C_4-C_{11}-O_{12}	125.21	125.09
C_4-C_{11}-O_{13}	111.36	112.58
O_{12}-C_{11}-O_{13}	123.43	122.33
C_{11}-O_{13}-C_{19}	120.54	123.71
C_{15}-C_{14}-C_{19}	119.36	119.11
C_{15}-C_{14}-H_{20}	121.33	121.42
C_{19}-C_{14}-H_{20}	119.31	119.47
C_{14}-C_{15}-C_{16}	120.64	120.60
C_{14}-C_{15}-H_{21}	120.56	120.37
C_{16}-C_{15}-H_{21}	118.80	119.03
C_{15}-C_{16}-C_{17}	118.89	119.04
C_{15}-C_{16}-C_{24}	118.17	118.20
C_{17}-C_{16}-C_{24}	122.83	122.68
C_{16}-C_{17}-C_{18}	120.95	120.78
C_{16}-C_{17}-H_{22}	120.05	120.29
C_{18}-C_{17}-H_{22}	118.98	118.92
C_{17}-C_{18}-C_{19}	118.95	118.86
C_{17}-C_{18}-H_{23}	120.65	120.73
C_{19}-C_{18}-H_{23}	120.40	120.41
O_{13}-C_{19}-C_{14}	116.65	116.89
O_{13}-C_{19}-C_{18}	122.02	121.43
C_{14}-C_{19}-C_{18}	121.19	121.59
C_{16}-C_{24}-O_{25}	119.91	119.28
C_{16}-C_{24}-C_{30}	120.11	121.15
O_{25}-C_{24}-C_{30}	119.98	119.57
C_{27}-C_{26}-C_{31}	120.04	119.98
C_{27}-C_{26}-H_{32}	120.05	120.12
C_{31}-C_{26}-H_{32}	119.92	119.89
C_{26}-C_{27}-C_{28}	119.95	119.97
C_{26}-C_{27}-H_{33}	120.04	120.03

Table 1. Theoretical optimized geometric parameters obtained from B3LYP/6-311++G(d,p) and HF/6-311++G(d,p) levels of theory for the title compound (continued)

C_{28}-C_{27}-H_{33}	120.01	120.00
C_{27}-C_{28}-C_{29}	120.09	120.06
C_{27}-C_{28}-H_{34}	120.13	120.19
C_{29}-C_{28}-H_{34}	119.79	119.76
C_{28}-C_{29}-C_{30}	120.29	120.29
C_{28}-C_{29}-H_{35}	119.62	119.43
C_{30}-C_{29}-H_{35}	120.08	120.27
C_{24}-C_{30}-C_{29}	122.59	122.49
C_{24}-C_{30}-C_{31}	118.11	118.17
C_{29}-C_{30}-C_{31}	119.19	119.26
C_{26}-C_{31}-C_{30}	120.42	120.43
C_{26}-C_{31}-H_{36}	120.92	120.67
C_{30}-C_{31}-H_{36}	118.65	118.89
C_{1}-O_{37}-C_{38}	120.61	125.14
O_{37}-C_{38}-O_{39}	123.74	122.79
O_{37}-C_{38}-C_{40}	112.05	113.14
O_{39}-C_{38}-C_{40}	124.21	124.07
C_{38}-C_{40}-C_{41}	124.98	124.50
C_{38}-C_{40}-H_{44}	113.17	113.32
C_{41}-C_{40}-H_{44}	121.85	122.18
C_{40}-C_{41}-H_{42}	120.83	120.81
C_{40}-C_{41}-H_{43}	121.59	121.93

4.2.3. Vibrational Frequencies

We performed a frequency calculation analysis to investigate the spectroscopic signature of p-benzophenoneoxycarbonylphenyl acrylate in this study. Vibrational frequencies were calculated by using B3LYP/6-311++G(d,p) and HF/6-311++G(d,p) methods. Table 2 shows the vibrational frequencies scaled by the factors [68,69] and experimental values, corresponding vibrational assignments with PED values, IR intensities and Raman activities of the compound, respectively. Scaled frequencies were compared with experimental values. It is found that all the compared data are found to be in good agreement with each other.

Table 2. Experimental and theoretical vibrational frequencies.

		Calculated frequencies (cm^{-1})					
		B3LYP 6-311++G(d, p)			HF 6-311++ G(d, p)		
[a]Assignment	Exp. (IR)	Scaled Freq.	IR intensity (km/mol)	R activity (Å4/amu)	Scaled Freq.	IR intensity (km/mol)	R activity (Å4/amu)
ν_{sym}^{3}(CH) (99)		3115	66.60	3.47	3047	106.06	2.56
ν_{sym}^{2}(CH) (99)		3094	55.34	0.30	3046	67.92	10.18
ν_{asy}^{4}(CH) (100)		3092	86.63	10.96	3038	73.77	2.19
ν_{sym}^{3}(CH) (85)		3091	80.78	2.48	3032	117.06	3.99
ν_{sym}^{2}(CH) (99)		3080	131.29	5.95	3026	84.51	5.31
ν_{sym}^{2}(CH) (92)		3077	100.41	4.03	3019	60.21	0.14
ν_{sym}^{1}(CH) (91)		3074	280.60	16.02	3018	184.69	10.02
ν_{asy}^{3}(CH) (93)		3071	7.92	2.16	3016	39.47	5.76
ν_{sym}^{1}(CH) (46)+ ν_{asy}^{2}(CH) (34)		3071	105.93	10.01	3010	159.87	7.01
ν_{asy}^{2}(CH) (84)+ ν_{sym}^{1}(CH) (16)		3068	35.59	3.53	3010	31.91	10.01
ν_{asy}^{2}(CH) (43)+ ν_{sym}^{1}(CH) (25)		3066	21.65	9.54	3008	127.14	4.52
ν_{asy}^{4}(CH) (99)		3065	169.29	5.67	3007	15.36	10.89
ν_{sym}^{1}(CH) (85)	3063	3061	105.38	40.44	2999	78.82	47.24
ν_{sym}^{1}(CH) (91)		3052	146.04	11.14	2989	122.48	12.28
ν_{sym}^{1}(CH) (87)		3043	47.85	0.21	2977	48.76	0.13
ν_{sym}^{4}(CH) (99)		3028	113.34	6.80	2960	104.59	7.22
ν^{4}(C=C) (45)+ ν(C_{38}=O_{39}) (33)	1741	1727	306.15	121.28	1694	135.40	334.28
ν(C_{11}=O_{12}) (73)	1730	1718	591.21	204.01	1661	148.03	331.61
ν(C_{38}=O_{39}) (40)+ ν^{4}(C=C) (26)+ ρr^{4}(HC) (10)	1651	1645	162.44	78.91	1624	120.33	197.57
ν^{2}(C=C) (16)+ ν^{1}(C=C) (10)		1615	2.74	7.99	1610	17.58	45.50
$\nu(ring)^{1}$ (45)+ $\nu(ring)^{2}$ (25)+ $\nu(ring)^{3}$ (15)+ ν(C_{24}=O_{25}) (10)		1579	538.91	43.06	1602	37.06	16.00
$\nu(ring)^{3}$ (25)+ $\nu(ring)^{2}$ (18)+ $\nu(ring)^{1}$ (10)		1575	874.65	228.11	1598	335.70	230.26
$\nu(ring)^{2}$ (16)+ δ^{2}(CH) (12)+ $\nu(ring)^{3}$ (10)	1599	1573	362.46	52.06	1595	136.11	14.56
ν(C_{24}=O_{25}) (17)+ $\nu(ring)^{2}$ (14)		1557	11.63	14.58	1571	3.94	16.15
$\nu(ring)^{2}$ (14)		1554	8.39	1.59	1569	6.80	0.27
$\nu(ring)^{3}$ (48)+ δ^{3}(CH) (11)		1551	455.97	157.19	1564	14.98	33.11
ν(C_{24}=O_{25}) (51)	1504	1475	13.53	77.44	1503	3.91	112.76
δ^{2}(CH) (50)		1471	1.71	33.67	1499	1.33	20.63
δ^{3}(CH) (50)+ ν^{3}(C=C) (11)	1446	1460	7.04	3.47	1483	0.45	6.18
δ^{1}(CH) (81)		1418	17.40	13.65	1434	2.46	17.21
ρr^{4}(HC) (83)		1386	34.21	37.55	1411	31.27	42.01
$\nu(ring)^{3}$ (37)+ δ^{3}(CH) (35)	1406	1384	4.71	12.95	1395	3.80	22.90
δ^{2}(CH) (37)	1305	1383	64.36	46.39	1391	6.18	23.59
δ^{1}(CH) (66)		1301	3.21	12.80	1328	2.31	14.86
δ^{2}(CH) (77)		1293	2.81	0.83	1310	0.46	6.61
τ^{3}(CH) (72)		1285	11.64	12.78	1309	4.83	10.27
$\nu(ring)^{1}$ (69)	1276	1281	47.43	45.18	1287	26.53	48.17
$\nu(ring)^{2}$ (48)+ κ^{4}(CH) (12)		1277	33.38	3.67	1275	21.79	82.02
κ^{4}(CH) (51)+ ν^{4}(C=C) (13)	1251	1274	28.31	11.10	1261	94.29	437.88
$\nu(ring)^{1}$ (38)+ δ^{1}(CH) (11)		1262	4.44	22.85	1246	131.23	1493.34
ν(C_{24}–C_{30}) (50)+ $\nu(ring)^{1}$ (12)	1207	1236	37.61	268.15	1213	1.46	7.02
ν(C_{4}–C_{11}) (35)+ δ^{3}(CH) (11)		1219	354.19	508.09	1208	9.07	217.22
ν(C_{38}–C_{40}) (30)+ ν(C_{38}–O_{37}) (15)+ δ(OCO) (13)+ δ^{4}(CCC) (13)+ δ^{4}(CH) (10)		1200	113.41	341.74	1202	32.35	390.82
ρr^{3}(CH) (40)+ ν(C_{1}–O_{37}) (12)+ $\nu(ring)^{3}$ (11)	1159	1181	54.84	132.92	1191	5.70	13.26
ρr^{2}(CH) (46)+ ν(C_{19}–O_{13}) (14)		1172	51.80	102.57	1184	0.30	45.80
ρr^{1}(CH) (67)+ $\nu(ring)^{1}$ (19)		1156	10.54	4.09	1174	2.51	3.45
ρr^{1}(CH) (63)	1111	1142	6.30	0.19	1165	7.16	58.13
ν(C_{11}–O_{19}) (19)+ δ^{2}(CH) (14)+ ρr^{1}(CH) (12)		1138	21.74	23.60	1162	45.73	273.00

Table 2. Experimental and theoretical vibrational frequencies (continued)

ρr^1(CH) (18)+ $\nu(C_{11}–O_{13})$ (11)		1133	475.66	842.44	1135	57.88	10.52
ν(ring)^1 (15)+ $\nu(C_{24}–C_{16})$ (15)		1121	1125.31	742.56	1126	4.46	11.46
ρr^3(CH) (49)+ ν(ring)^3 (15)+ ρr^2(CH) (12)	1076	1088	4.53	23.79	1091	1.64	4.18
ρr^2(CH) (44)+ ρr^3(CH) (13)+ ν(ring)^3 (10)		1087	4.67	6.86	1088	0.62	1.58
ν(ring)^1 (45)+ ρr^1(CH) (14)		1062	4.68	11.66	1063	0.09	9.87
$\nu(C_{11}–O_{19})$ (19)+ $\nu(C_{11}–O_{13})$ (18)+ δ(OCO) (10)		1035	25.00	182.61	1054	8.45	108.01
δ^1(CCC) (26)+ ν(ring)^1 (25)+ ρr^1(CH) (17)		1009	12.18	5.10	1052	6.89	23.84
δ^2(CCC) (34)+ ρr^1(CH) (14)+ δ(CCO) (12)	1014	994	1.97	7.97	1027	0.37	0.30
δ^3(CCC) (48)+ δ^4(CCH) (20)		991	13.98	53.45	1018	5.68	222.51
κ^4(HCCH) (94)		988	2.66	0.96	1017	1.22	6.44
w^4(CH) (48)+ $\nu(C_{38}–O_{37})$ (10)		986	62.81	588.42	1016	0.22	3.00
w^1(HCCC) (70)		977	2.78	79.09	1011	0.19	4.19
w^3(HCCC) (70)		971	0.62	2.18	1008	3.10	5.82
ξ^4(HCCH) (95)		970	0.64	65.35	1006	0.12	6.98
ν(ring)^1 (47)+ δ^1(CCC) (27)		958	55.77	28.68	1004	0.14	53.85
κ^1(HCCC) (53)+ κ^2(HCCC) (12)	979	957	0.91	1.89	997	1.20	44.99
κ^2(HCCC) (35)+ κ^1(HCCC) (22)	968	952	2.01	16.87	992	2.09	0.96
κ^3(HCCC) (70)	943	943	0.87	0.19	991	1.84	11.66
κ^2(HCCC) (58)	927	940	3.29	4.13	983	49.98	7.88
w^1(HCCC) (81)		921	0.72	8.42	974	8.75	1.55
δ(OCC) (26)		902	3.80	123.52	910	6.15	88.73
ξ^3(HCCH) (71)		880	0.25	55.89	895	1.49	47.21
$\nu(C_{37}–C_{38})$ (20)+ $\nu(C_{38}–C_{40})$ (19)+ ν(ring)^3 (12)		861	0.29	28.90	891	7.67	74.41
ξ^2(HCCH) (18)+ x^2 (CCOC) (15)	855	840	2.14	39.23	877	1.44	2.09
w^1(HCCC) (86)	852	830	6.45	7.35	862	3.60	14.31
w^3(HCCC) (79)		820	1.82	9.41	857	1.10	5.47
w^2(HCCC) (89)	823	808	6.58	4.67	856	0.22	1.95
ν(ring)^2 (13)+ $\nu(C_{13}–O_{11})$ (17)		806	13.62	15.25	826	10.82	4.41
ξ^1(HCCH) (25)+ x^1(OCCC) (15)	796	801	5.04	9.79	813	2.09	3.05
$\nu(C_{13}–O_{11})$ (18)+ ν(ring)^2 (12)	786	795	91.22	5.09	795	47.86	11.00
w^4(HCCC) (79)+ x(OCOC) (15)		786	7.53	26.62	792	23.19	41.36
δ(OCO) (21)+ $\nu(C_1–O_{37})$ (17)	758	772	2.93	3.18	783	5.28	12.19
w^2(CCCC) (10)		744	14.05	59.70	753	17.36	7.58
x(OCOC) (27)+ x^4 (CCCC) (15)	731	726	5.18	3.62	747	3.01	88.86
ξ^1(HCCH) (38)		691	10.33	56.44	710	3.94	59.01
δ^1(CCC) (11)	690	682	3.89	8.02	696	4.59	16.21
δ^1(CCC) (11)+ x^1(OCCC) (11)		678	7.69	22.34	688	1.16	6.56
x^1 (OCCC) (11)		669	2.46	44.87	680	0.58	38.20
x (OCOC) (47)		657	0.61	25.29	666	1.62	47.27
δ^3(CCC) (46)		623	3.62	4.21	636	6.60	2.19
δ^3(CCC) (41)		620	16.19	5.91	633	10.73	3.53
δ^1(CCC) (58)+ δ^3(CCC) (12)		608	6.11	0.83	620	6.55	1.28
δ^1(CCC) (13)+ δ(OCC) (11)		606	0.86	9.97	615	1.01	11.65
δ(C–CO–C) (25)		555	18.01	2.25	568	8.91	5.50
δ(OCC) (34)+ $\nu(C_{38}–C_{40})$ (18)		547	2.88	3.92	553	1.45	4.71
δ^4(CCC) (19)+ δ(C–CO–C) (10)		506	22.16	4.94	515	1.51	1.17
x^3(OCCC) (31)		498	0.61	6.71	509	4.17	7.16
x^2(OCCC) (23)		489	1.89	4.52	498	3.08	7.24
w^2(HCCC) (44)+ x(OCOC) (39)		477	5.63	0.75	486	3.77	13.56
w^1(CCCC) (18)+ δ(OCC) (10)		456	0.08	3.16	464	0.45	7.49
w^1(CCCC) (29)		421	0.46	5.64	433	0.38	8.34
w^1(CCCC) (31)		411	1.37	0.47	429	0.51	0.71
w^3(CCCC) (39)+ κ^3(HCCC) (13)		407	0.03	0.03	424	0.17	0.83
w^1(CCCC) (53)+ κ^2(HCCC) (16)		398	1.13	0.39	417	0.53	0.09
δ(OCC) (26)+ $\nu(C_{24}–C_{16})$ (12)		392	1.64	6.36	394	0.62	8.21
δ(OCC) (40)		372	1.38	5.12	377	2.14	2.53

Table 2. Experimental and theoretical vibrational frequencies (continued)

δ(OCC) (24)+ w^2(CCCC) (21)+ w^1(CCCC) (11)	358	0.90	0.41	351	1.36	5.51
δ(OCC) (27)+ δ(CC–CO) (20)+ δ^4(CCC) (12)	321	0.24	15.96	329	3.26	2.79
δ^4(CCC) (35)+ δ(CC–CO) (12)	311	4.70	6.75	314	1.09	28.17
x^3(CCCC) (20)+ x^3(OCCC) (11)	291	10.89	3.50	299	3.54	4.50
δ^2(CCC) (15)+ ν(C_{24}–C_{16}) (12)+ δ(C–CO–C) (10)	245	0.90	1.23	250	1.62	2.04
δ^2(CCC) (17)+ δ(OCC) (11)	214	0.99	2.34	216	0.45	2.71
w^1(CCCC) (25)+ δ^2(CCC) (16)	197	5.05	0.90	201	7.41	3.81
δ(CC–CO) (16)+ δ(OCC) (15)+ δ^2(CCC) (10)	177	2.93	2.49	179	1.16	1.15
δ(OCC) (12)+ ν(C_{13}–O_{11}) (10)	146	2.05	2.26	146	2.46	8.00
w^4(CCOC) (17)	132	2.06	5.76	134	2.55	0.20
w^4(CCCO) (64)	121	4.36	0.48	131	4.33	1.03
δ(COC) (42)+ δ(CC–CO) (14)	113	0.67	0.97	119	2.49	1.52
w^1(CCCC) (13)+ w^2(CCCC) (10)	90	1.82	0.39	93	1.28	0.68
w^2(CCCC) (41)+ w^1(CCCC) (19)	72	10.97	0.33	73	6.39	0.15
w^2(OCCC) (54)+ w^1(CCCC) (10)	63	2.36	1.63	62	2.34	1.40
w^2(CCCC) (11)	55	6.39	0.03	55	6.50	0.54
w^3(OCCC) (36)+ x^3(OCCC) (31)+ w^2(CCCC) (21)	48	0.49	0.65	49	1.76	1.08
w^2(CCCC) (39)+ x^4(OCOC) (39)	38	2.89	0.68	37	1.84	0.34
w^2(OCCC) (11)+ δ(CC–CO) (11)	32	0.99	0.47	26	2.42	0.48
w^3(COCC) (38)	18	0.93	1.19	17	1.29	0.50
w^2(OCCC) (48)+ w^3(CCCC) (10)	14	0.42	1.10	12	2.65	2.53
w^1(CCCC) (53)+ w^3(CCCC) (19)	12	1.31	2.36	8	0.76	3.16

Abbreviations used: ν: stretching; δ: bending; ς: rocking; τ: torsion; sym: symmetric; asy: asymmetric; ρr: scissoring; w: wagging; κ: twisting; x: out of bending.

[a] : PED less than 10% are not shown

[1] Ring-1

[2] Ring-2

[3] Ring-3

[4] Vinyl

The existence of aromatic rings in a structure can easily be determined owing to the relation of (C–H) and (C=C–C) ring vibrations. The (C–H) stretching occurs above 3000 cm−1 and is typically exhibited as a multiplicity of weak to moderate bands, compared with the aliphatic (C–H) stretch [70]. In 1994, Roeges showed that, the (C–H) stretching vibrations of the phenyl ring are expected in the region 3000–3120 cm^{-1} [71]. According to Klots and Collier [72], the stretching vibration modes were reported at 3085, 3074, 3065 and 3045 cm^{-1} bands for benzoxazole. In the current compound, the observed peak at 3063 cm^{-1} can be assigned to the C–H stretching mode of the aromatic group in the BPOCPA. The theoretical IR values

corresponding to the IR frequency observed are calculated to be about 3028–3115 cm^{-1} at B3LYP/6-311++G(d,p) and 2960–3047 cm^{-1} at HF/6-311++G(d,p) basis sets, respectively. Among the C–H stretching bands, the calculated peak at 3074 cm−1 with the assignment of νsym^{1}(CH) (91) has the highest IR intensity in Table 2. As for the carbon-carbon modes, the benzene ring possesses six–ring stretching vibrations observed near 1440, 1490, 1580 and 1600 cm^{-1} for the highest wave numbers. The others start 12 to be active at 1000 and 1315±65 cm^{-1} bands [73]. In BPOCPA under C1 symmetry, the (C=C) stretching bands were changed from 795 to 1579 cm^{-1} at B3LYP/6-311++G(d,p) and from 795 to 1602 cm^{-1} at HF/6-311++G(d,p) calculation level while these IR bands are identified at 796–1599 cm^{-1}. Here, the IR value lying at 1121 cm^{-1} is attributed to very intense band stemming from the strong electron–donor group attached to benzene ring [70]. Moreover, the C=C stretching vibration is used to determine the degree of conjugation through the π–electron chain [74]. For this study, the simultaneous activation of C=C stretching modes belonging to the BPOCPA (1274–1727 cm^{-1} and 1261–1694 cm^{-1} at B3LYP/6-311++G(d,p) and HF/6-311++G(d,p), respectively) in the IR spectra confirms the charge transfer inter action between the donor and acceptor groups through the π–system [75]. The characteristic C–C stretching bands of the compound are computed in the vibration range of 245–1236 cm^{-1} at B3LYP/6-311++G(d,p) level(250–1213 cm^{-1} for HF/6-311++G(d,p)). In these modes, the greatest IR intensity value is computed to be about 91.22 km/mol for the C_{38}–C_{39} stretching vibration. The wavenumber difference between C–C and C=C stretching vibrations may be related to the presence of the electron engagement in the C=C vibration modes. In addition, the absorption peaks at 1741 and 1730 cm^{-1} are characteristic of C=O stretching vibrations of carbonyl groups. As seen from Table 2, the strong IR

band identified at 1651 cm^{-1} is assigned to C=O ketone stretching vibrations of the pendant benzophenone moiety. Theoretically, the (C=O) stretching bands are calculated to be about 1727–1475 cm^{-1} at B3LYP/6-311++G(d,p) calculation level and 1503–1694 cm^{-1} at HF/6-311++G(d,p). In the compound under C_1 symmetry, the IR bands identified at 1200–146 cm^{-1} are assigned to C–O stretching vibrations. Further, the calculated band at 1557(1571) cm^{-1} can be ascribed to C_{24}=O_{25} stretching mode obtaining the highest IR intensity value among the carbon=oxygen modes. Similarly, the calculated peak at 1219(1208) cm^{-1} in IR spectra can be attributed to the C–O stretching mode with the largest IR intensity value. On the other hand, the bands due to C–H in–plane bending vibrations interacting some what with C–C stretching vibrations are determined as a number of IR bands in the region 986–1645(1016–1624 at HF/6-311++G(d,p)) cm^{-1} at B3LYP/6-311++G(d,p). The similar results can be found in the literature[76]. The other bands calculated at 12–1645(8–1624) cm^{-1} for the title compound are assigned to the bending vibrations such as torsion, scissoring, wagging, twisting and umbrella forming the skeletal structure. The maximum IR intensity value of 354.19 km/mol is noted at 1219 cm^{-1} for the CH bending mode in the ring[3] in Table 2.

4.2.4. Thermodynamic Properties

Several thermodynamic parameters performed by B3LYP and HF with 6-311++G(d,p) level of theory are given in Table 3. Scale factors are recommended [77] for an accurate prediction in determining the zero–point vibration energies. The total energies and changes in the total entropy of the compounds at room temperature are depicted at different theoretical methods. Table 3 indicates several thermodynamic parameters of the molecule without experimental determinations. It

is apparent from the table 3 that all the calculations are close to each others. For the energy parameters such as total and zero–point vibrational energy, the calculations obtained from B3LYP/ 6-311++G(d,p) level of theory are smaller than those of HF/ 6-311++G(d,p) basis set as a result of the presence of electron correlation in the calculation steps. Namely, the total energy (zero–point vibrational energy) values are found to be about -1262.517 (205.113) and -1254.369 (224.693) au, respectively. Moreover, computations of HF/6-311++G(d,p) basis set for rotational constants are generally smaller than B3LYP ones. On the other hand, the thermal energy values calculated from HF method are obtained to be larger than those of B3LYP. Additionally, the dipole moment, which is an important quantity explaining the electronic property of a molecule, stems from non-uniform distribution of charges on the various atoms in the molecule and is mainly used to study the intermolecular interactions involving the van der Waal type dipole–dipole forces, etc., because the larger dipole moment, the stronger intermolecular interactions appears [78]. Hence, we can easily define the biological characteristics especially related to the interaction with enzyme active sites of the molecules. The dipole moment value belonging to the molecule studied is computed to be about 3.242 Debye for the HF/6-311++G(d,p) basis set and 3.120 Debye for B3LYP /6-311++G(d,p) level of calculation. This may be attributed to the fact that the title compound obtains higher polarity (non-uniform distribution of charges on th various atoms) enough to bond metallically. This result is also favored by the evidences of other parts.

Table 3. Thermodynamical properties of BPOCPA

Parameters	**BPOCPA(HF)**	**BPOCPA(DFT)**
Total energy	-1254.3689	-1262.5166
Zero–point vibrational energy	224.693	205.1126
	0.77397	0.78503
Rotational constant	0.04494	0.04374
	0.04315	0.04172
Entropy		
Total	170.468	176.390
Translational	43.635	43.635
Rotational	36.614	36.660
Vibrational	90.220	96.095
Heat capacity		
Total	82.619	89.469
Translational	2.981	2.981
Rotational	2.981	2.981
Vibrational	76.658	83.507
Thermal Energy		
Total	238.579	224.015
Translational	0.889	0.889
Rotational	0.889	0.889
Vibrational	236.802	222.238
Dipole Moment		
μ_x	3.1989	-3.0496
μ_y	0.5263	0.6582
μ_z	-0.0286	0.0255
μ	3.2420	3.1199

4.2.5. HOMO-LUMO Analyses

As well known, highest occupied molecular orbital (HOMO) and lowest unoccupied molecular orbital (LUMO) play a crucial role to determine the optical and electrochemical properties of an organic compound as well as in UV–Vis spectra and chemical reactions [79]. The interaction between the species can be interpreted with the aid of HOMO and LUMO information of the compound. The former is the outermost orbital containing electrons and tends to give these electrons such as an electron donor. On the other hand; the latter is the innermost orbital containing free places to accept electrons [80]. According to the molecular orbital theory, the

transition of $\pi - \pi^*$ stems from the interaction between HOMO and LUMO orbital of the title compound [81]. Thereby, the HOMO energy is directly attributed to the ionization potential while the energy of the LUMO is directly related to the electron affinity [82]. In other words, the energy difference between HOMO and LUMO orbital is described as energy gap that is an important stability for the structures [83]. 3D plots of the HOMO and LUMO belonging to the BPOCPA monomer are shown in Figure 14. It is apparent from the fig. 14 that both the HOMOs and LUMOs are mostly π-antibonding-type orbitals. The former orbitals are mostly delocalized on the vicinity of the benzene rings but no translation appears on vinylic and carbonyl groups. In contrast, the latter orbitals are localized mainly on the title compound expect for the hydrogen atoms. Moreover, the HOMO and LUMO energies of the title compound were -6.87 eV and -2.47 eV respectively at B3LYP/6-311++G(d,p) basis set. The value of the energy separation between the HOMO and LUMO (energy band gap) is found to be about 4.40 eV (Table 4). This is attributed the fact that the title structure is quite stable. Additionally, in previous work, we studied on the characterization of the title compound, p-biphenyloxycarbonylphenyl acrylate. It was observed that the HOMO value is found to be about -6.21 eV when the optical band gap is obtained to be about 4.76 eV at B3LYP/6-311++G(d,p) level of calculation. Based on the findings obtained (lower band gap and greater HOMO values), the electronic donor ability of the p-benzophenoneoxycarbonylphenyl acrylate (the present compound) is stronger than the p-biphenyloxycarbonylphenyl acrylate (the studied molecule) due to the different number of the carbonyl groups in the title compounds studied [84].

Besides, the ionization potential and electron affinity values allow us to determine the other important quantities such as electronegativity (χ), hardness (η),

softness (ζ), and electrophilicity index (ψ) for the potential technological and industrial applications of an organic compound. The data obtained are depicted in Table 4. According to the table 4, the χ and ψ values are found to be about 4.67 and 4.96 eV, respectively. This may be in accordance with the fact that although the title structure has possible sites for the electrophilic attack (being favored by the MEP analysis) the organic compound is quite stable (being supported by the frontier orbital examination). Whereas the η value is also obtained to be about 2.20 eV, the ζ of 0.23 eV^{-1} is observed for the compound studied, presenting that the monomer synthesized may be useful in the optic and opto-electronic applications [85-87].

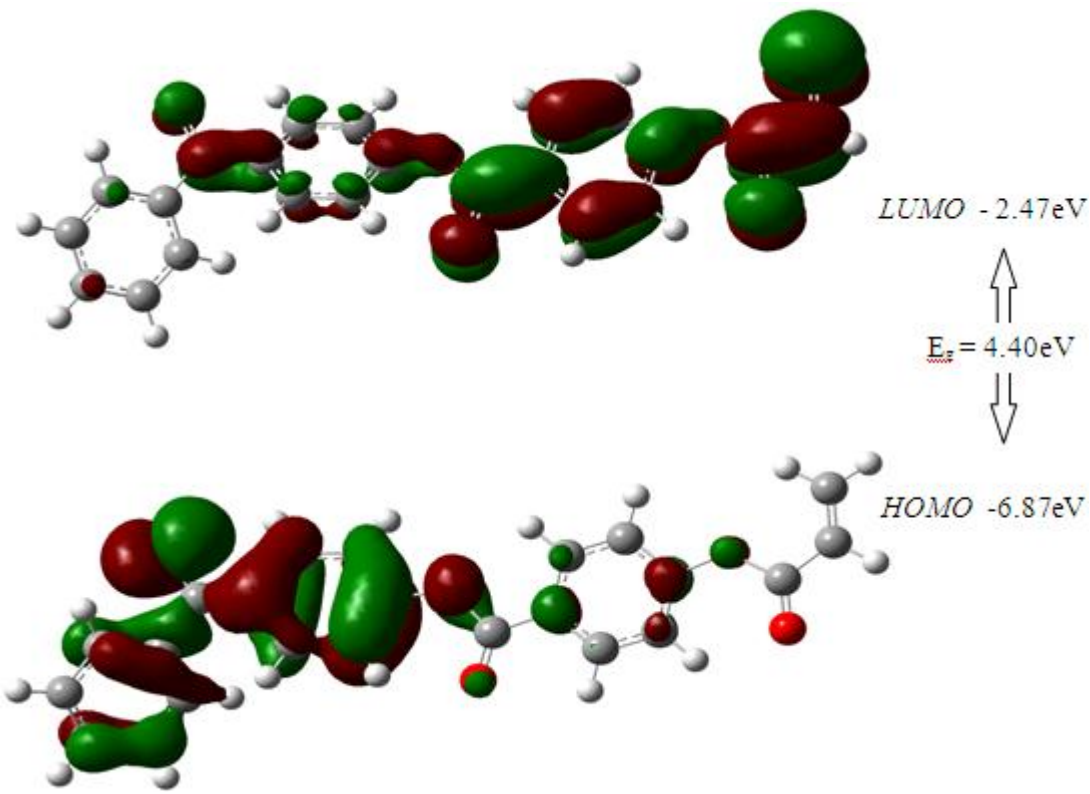

Figure 14. 3D maps of the HOMO and LUMO of BPOCPA (Positive phase is shown by red regions while negative phase is displayed by green blobs).

4.2.6. MEP and ESP Analyses

Molecular electrostatic potential (MEP) and electrostatic potential (ESP) being useful characteristics to demonstrate the charge distributions of an organic compound gives the information about how the molecules interact with another molecule. The molecular electrostatic potential, V(r), is known as the interaction energy between the electrical charge generated from the electrons and nuclei of the molecule studied and a positive test charge to be located at a given point r(x, y, z) [88,89]. MEP is also a very useful descriptor to determine the sites in the molecule for electrophilic attack and nucleophilic reactions as well as hydrogen-bonding interactions as a consequence of the relation with the electronic density [90-92]. Fig. 15 shows 3D plots of the MEP belonging to the BPOCPA. Here, electrophilic reactivity is presented by negative (red) regions whereas nucleophilic reactivity is shown by the positive (blue) regions.

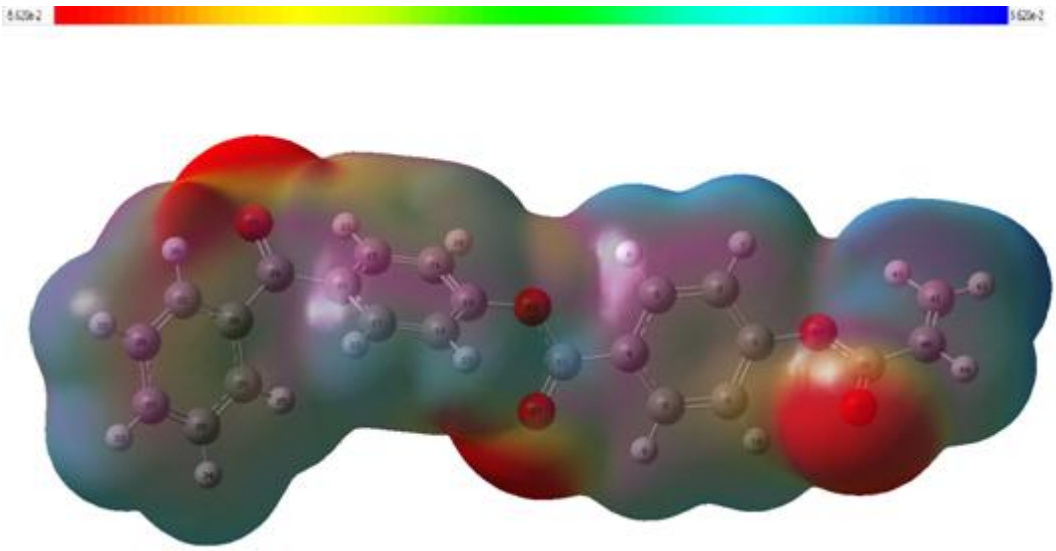

Figure 15. 3D map of the molecular electrostatic potential (MEP) map of BPOCPA (Red color depicts the negative regions while blue color illustrates the positive regions of MEP).

It is obvious from the fig. 15 that for the electrophilic attack there are three possible sites on the compound synthesized in this work. These red (negative) regions are delocalized on the oxygen atoms of the carbonyl groups. These regions reflect the most electronegative region (excess negative charge). As for the blue regions in the fig. 15, the nucleophilic reactivity of the molecule is localized on the hydrogen atoms. The compound studied is, in this respect, useful to both bond metallically and interact intermolecularly. Whereas there are two greater negative regions for p-biphenyloxycarbonylphenyl acrylate molecule in the previous study, p-benzophenoneoxycarbonylphenyl acrylate obtains three main negative regions as a consequence of the strong electronic donating carbonyl groups. This is associated with the fact that the latter compound is more useful for the intermolecular interactions. Furthermore, Fig. 16 pictures the electrostatic potential (ESP) fig. 16 belonging to the BPOCPA compound. It is apparent from the fig. 16 that the most negative ESP being reflected as a yellowish blob is spread more over the oxygen atoms, presenting not only the delocalization of π-electrons over the carbonyl groups but also the extended conjugation of the vinylic and benzene rings with these groups. On the other hand, the positive ESP is localized on the rest of the organic compound, meaning that the ESP map correlates with electronegativity and partial charges in the structure synthesized in this work. Moreover, the total charge density contour is given in the fig. 16. As seen from the fig. 16, generally the reddish and yellowish colors are found to be the predominance on the molecule as a consequence of the negative charge distribution.

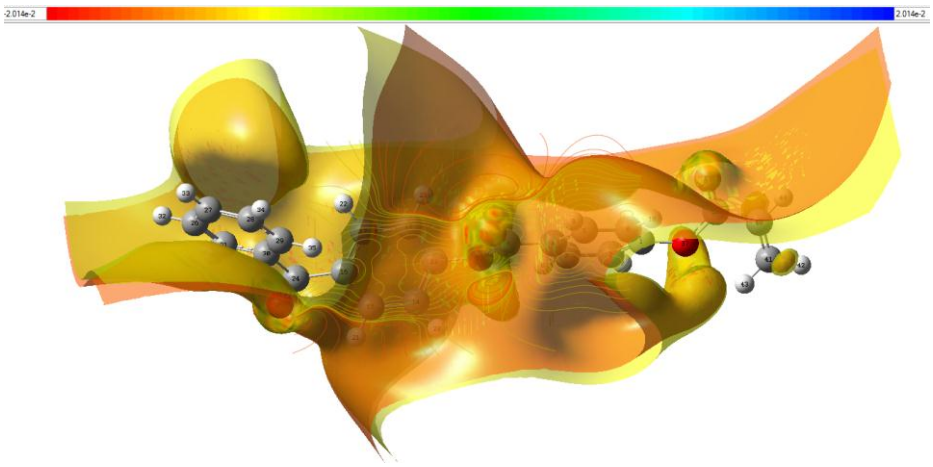

Figure 16. 3D map of the electrostatic potential (ESP) of BPOCPA.

Table 4. Calculated energy values in the ground state with singlet symmetry at B3LYP/6-311++G(d,p) level of theory for the potential technological and industrial applications

Quantity	Value
Lowest MO Eigen value (eV)	–522.53
Highest MO Eigen value (eV)	1357.94
HOMO (eV)	-6.87
LUMO (eV)	-2.47
HOMO–LUMO gap (eV), $\lvert \Delta E \rvert$	4.40
χ (electronegativity) (eV)	4.67
η (chemical hardness) (eV)	2.20
ζ (Softness) $(eV)^{-1}$	0.23
ψ (Electrophilicity index) (eV)	4.96

4.2.7. UV-Visible Spectra Analyses

Classification of the electronic transitions is usually conducted with regard to the orbitals engaged or to specific parts of the molecule involved. As well known that π(donor)–π*(acceptor) and n–π* are the common types of electronic transitions in an

organic compound [93,94]. The former transition is attributed to the weak transition while the latter one is related to the strong transition. In the current study, both experimental and theoretical electronic absorption spectra are obtained to define the electronic transitions of the title compound studied and compared with each other. The experimental and computed electronic values, such as Singlet-A, absorption wavelength, excitation energies, transitions and oscillator strengths are listed in Table 5. It is visible from the table 5 that the absorption bands belonging to the BPOCPA are experimentally centered at 310, 344 and 368 nm in the solution of THF. Here, the absorption wavelength λ_{max} of the BPOCPA is observed at 344 nm due to the effective π–π* conjugated segments in the title compound such as the C=C and vinylic group. The peak calculated in 344 nm is related to the overlapping of π-π* transition in benzene ring and oscillation effect whereas the weak absorption peak at 368 nm stems from the $n \rightarrow \pi^*$ type transition in the carbonyl groups. On the other hand, the absorption maxima defined as the functions of the electron availability are calculated to be about 289, 311, and 341 nm at the TD-B3LYP/6-311++G(d,p) and 217, 225 and 271 nm at the TD-HF/6-311++G(d,p) level of theory [95-97] in the vacuum. Based on the results obtained, the calculation results are found to be shorter than the experimental evidences as a consequence of the calculations to be performed in the gas phase without considering the solvent effect [98]. It is attributed to the fact that the calculated energy transitions are blue shifted from the experimental findings. However, the agreement between theoretical (especially TD-B3LYP/6-311++G(d,p) basis set) data and experimental results is quite acceptable. The percentage contribution of the translations evaluated from the Singlet-A values (CI expansion coefficients) is also another important result obtained from Table 5. The visible absorption maxima of the molecule synthesized are in accordance with the electron

transition between frontier orbitals (such as translation from HOMO to LUMO; or HOMO-1 to LUMO+1). The experimental bands observed at 310 and 344 nm may be attributed to the transition of HOMO-1 → LUMO(%60.75) and HOMO → LUMO(%48.54), respectively. Likewise, the experimental band found at 368 nm may be assigned to a transition from HOMO-1 → LUMO+1. It is noted that other one-electron excitations may also contribute to describe this observed band [99]. Oscillator strength values are also displayed in Table 5. As seen from the table 5 that the lowest intense band is observed to be about 0.0078 and 0.0024 at TD-B3LYP/6-311++G(d,p) and TD-HF/6-311++G(d,p) calculation levels, respectively. According to the oscillator strength calculated, the least intense band centered at 368 nm is due to the partly forbidden n– π* transition.

Table 5. Experimental and Theoretical electronic absorption spectra values of BPOCPA

Excitation Excited state 1		**Singlet-A**		**Wave Length (nm)**			**Oscillator Strength (f)**		**Translation**	
TD–B3LYP/6-311++G(d,p)	TD–HF/6-311++G(d,p)	TD–B3LYP/6-311++G(d,p)	TD–HF/6-311++G(d,p)	Exp.	TD–B3LYP/6-311++G(d,p)	TD–HF/6-311++G(d,p)	TD–B3LYP/6-311++G(d,p)	TD–HF/6-311++G(d,p)		
93 → 99	90→98	-0.17432	0.19304	368	341	271	0.0078	0.0024	HOMO-4→LUMO+1	HOMO-7→LUMO
93 →100	90→99	0.12383	-0.45351						HOMO-4→LUMO+2	HOMO-7→LUMO+1
96 → 98	90→100	0.17555	-0.28067						HOMO-1→LUMO	HOMO-7→LUMO+2
96 → 99	90→114	0.36837	-0.15307						HOMO-1→LUMO+1	HOMO-7→LUMO+16
Excited state 2										
96 → 98	92 →102	0.28317	-0.17408	344	311	225	0.4984	0.7664	HOMO-1→LUMO	HOMO-5→LUMO+4
96 → 99	94 → 98	0.12301	-0.27675						HOMO-1→LUMO+1	HOMO-3→LUMO
97 → 98	94 → 99	0.61462	-0.10355						HOMO→LUMO	HOMO-3→LUMO+1
Excited state 3										
95 → 98	92 →102	0.11389	0.17864	310	289	217	0.1697	0.0117	HOMO-2→LUMO	HOMO-5→LUMO+4
96 → 98	93 →101	0.57190	-0.14121						HOMO-1→LUMO	HOMO-4→LUMO+3
97 → 98	93 →104	-0.25397	0.14533						HOMO→LUMO	HOMO-4→LUMO+6
97 → 99	94 → 98	0.21459	0.35521						HOMO→LUMO+1	HOMO-3→LUMO

Abbreviations used: [a]: DMSO

4.2.8. Atomic Charges

As well known, the effective atomic charges to be inferred from the quantum mechanical calculations play an important role for the identification of the molecular systems. Moreover, with the aid of the charge distribution of a molecule, the vibrational spectra belonging to the compound can be estimated sufficiently [100]. In the current study, the charge distributions calculated by the Mulliken [101,102] at the B3LYP/6-311++G(d,p) and HF/6-311++G(d,p) calculation levels for the equilibrium geometry of the monomer BPOCPA are illustrated in Table 6. It is visible from the table 6 that the magnitudes of the carbon atomic charges for the compounds are found to be both positive and negative at each basis set. The magnitudes are obtained to be in a range from -0.248 to 0.483 and -0.273 to 0.721 at the B3LYP/6-311++G(d,p) and HF/6-311++G(d,p) basis sets, respectively. The positive charges on C_1, C_{11}, C_{19} and C_{38} stem from the presence of the high electronegative (negatively charged) oxygen atoms being closer to these atoms. In fact the highest atomic charge value of 0.483 (0.721) is for C_{11} atom due to the two oxygen atoms. Additionally, in the title compound BPOCPA the Mulliken atomic charge of C_{41} and C_{40} being from the member of Vinylic group becomes more negative such as -0.248 and -0.273 at the B3LYP/6-311++G(d,p) and HF/6-311++G(d,p) basis sets, respectively. This is attributed to the fact that nature of the Vinylic group withdraws the electron as a consequence of the resonance [103]. As for oxygen atomic charges, the magnitudes are calculated from -0.561 to -0.360 and from -0.761 to -0.483 at the B3LYP/6-311++G(d,p) and HF/6-311++G(d,p) levels of theory, respectively. In other words, all the oxygen atoms attached to the carbons exhibit the negative charges (acceptor feature) due to the excess electron density. Here, the Mulliken atomic charge corresponding to the O_{13} atom is noted to be more negative due to the high positive

charge resulted from the carbon atoms. Moreover, the magnitudes of the hydrogen atomic charges are obtained to be only positive values (acceptor feature), indicating the charge transfer from hydrogen to carbon atom. The major conclusions to be derived from the atomic charge analysis are as follows:

*All the hydrogen atoms in the molecules lose electrons,

*Carbon atomic charges are found to be both positive and negative values according to the position in the title compound.

*Charge migration to heavy atoms can be related to molecular interactions for the molecule.

*All the oxygen atoms in the monomer accept electrons.

*The negatively charged lone pair confirms that charge is transferred from hydrogen to carbon atoms.

Table 6. Mulliken atomic charges of BPOCPA

ATOM NO	BPOCPA atomic charges(DFT)	BPOCPA atomic charges(HF)
1 C	0.260	0.389
2 C	-0.217	-0.228
3 C	-0.017	-0.029
4 C	-0.197	-0.241
5 C	-0.088	-0.092
6 C	-0.113	-0.129
7 H	0.182	0.193
8 H	0.191	0.215
9 H	0.192	0.217
10 H	0.230	0.217
11 C	0.483	0.721
12 O	-0.367	-0.497
13 O	-0.561	-0.761
14 C	-0.170	-0.182
15 C	-0.116	-0.124
16 C	-0.092	-0.136
17 C	-0.099	-0.109
18 C	-0.112	-0.133
19 C	0.255	0.391
20 H	0.180	0.191
21 H	0.185	0.209
22 H	0.189	0.203
23 H	0.213	0.201
24 C	0.181	0.382
25 O	-0.359	-0.483
26 C	-0.157	-0.174
27 C	-0.120	-0.126
28 C	-0.176	-0.190
29 C	-0.080	-0.099
30 C	-0.110	-0.151
31 C	-0.106	-0.122
32 H	0.158	0.171
33 H	0.158	0.171
34 H	0.157	0.171
35 H	0.188	0.204
36 H	0.183	0.206
37 O	-0.550	-0.743
38 C	0.475	0.694
39 O	-0.372	-0.497
40 C	-0.201	-0.273
41 C	-0.248	-0.226
42 H	0.176	0.182
43 H	0.197	0.211
44 H	0.194	0.206

4.2.9 NMR Spectra Analyses

In the current work, both experimental and theoretical chemical shifts are determined and compared with each others in order to obtain the practical information on the chemical structure and conformation of the title compound studied. We record only ^{1}H-NMR chemical shifts of the monomer BPOCPA in the DMSO solution. Fig. 17 displays the ^{1}H-NMR spectra belonging to the BPOCPA. The proton shifts extracted from the fig. 17 are pictured in Figure 18 clearly. It is visible from the fig. 17 that ^{1}H isotropic chemical shift values are observed at 6.45–8.21 ppm (Table 7). There is doublet at δ 6.1 ppm (minimum value) corresponding to Hb proton of vinylic group and one quartet at δ 6.45 ppm corresponding to vinylic Ha proton. Moreover, the doublet observed at δ 6.6 ppm is responsible for Ha-Hc trans coupling of vinylic group. The five doublets found at δ 7.45, 7.50, 7.76, 7.86 and 8.21 ppm are peculiar to Hd, Hf, He, Hg, Hh proton, being related to the single O-coupling of the C_6H_4-groups in structure. The two triplets at δ 7.57 and 7.68 ppm are attributed to Hj and Hi protons obtaining the double O-coupling of C_6H_4-groups in the structure. It is another interesting point obtained from Figure 17 that no impurities could be noticed from the 1H NMR spectra for the monomer synthesized. Additionally, the computed ^{1}H chemical shifts in the DMSO solution are given in Table 7.

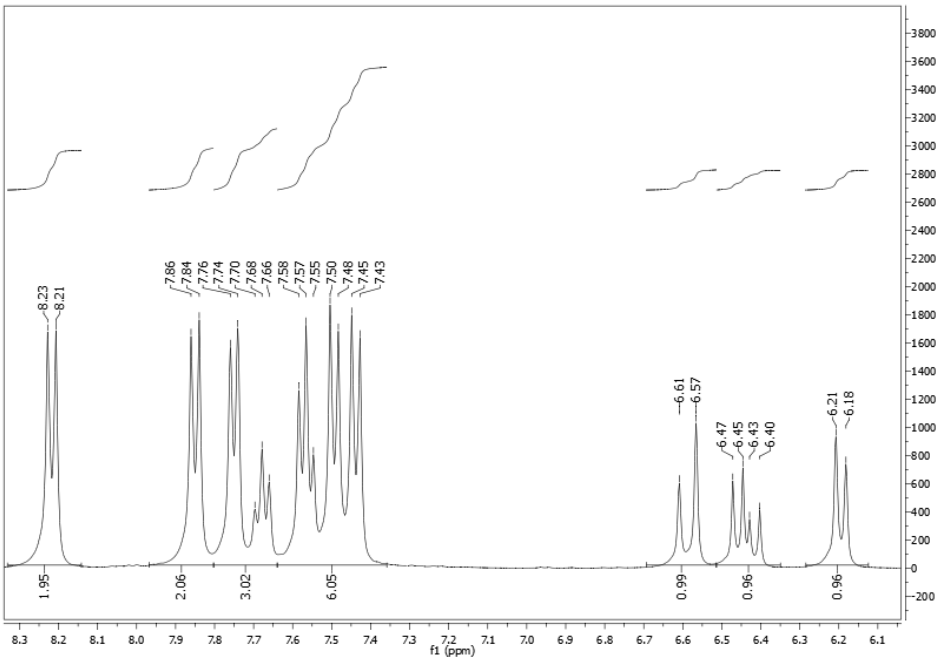

Figure 17. Experimental 1H-NMR Spectra of BPOCPA.

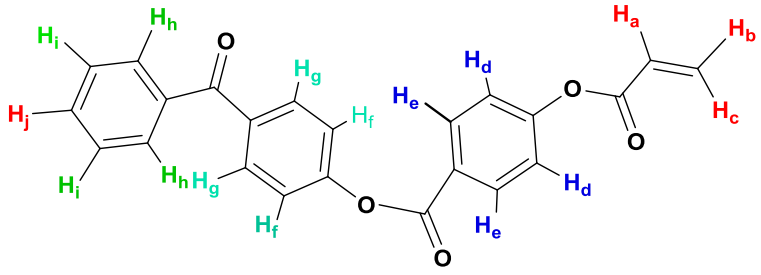

Figure 18. Proton scheme of BPOCPA.

As well known, the isotropic chemical shift values deduced from the NMR analysis are useful parameters to determine the relative ionic species and calculate reliable magnetic properties depicting the accurate predictions of molecular geometries [104]. In the present study, the full geometry optimization of the title compound is carried out using HF and B3LYP methods. Then, GIAO ^{1}H and ^{13}C chemical shift values are calculated by the same methods with 6-311++G(d,p)

calculation level in the vacuum. The isotropic shielding values computed are used to find the isotropic chemical shifts δ with regard to tetramethylsilane (TMS) as the following relation:

$$\delta_{iso}^{X} = \sigma_{iso}^{TMS} - \sigma_{iso}^{X} \quad (52)$$

The results obtained are also gathered in Table 7. It is apparent from the table 7 that the ^{1}H-NMR calculations obtained at B3LYP/6-311++G(d,p) level of theory are in better agreement with the experimental findings as compared to those of HF/6-311++G(d,p) basis set. This may be attributed to the fact that no electron correlation effects are taken into account in HF methods whereas the B3LYP methods including the electron correlation effect treat the electronic energy as a function of the electron density of all the electrons in the material simultaneously [105]. The values of ^{1}H isotropic chemical shift are observed in the range of 6.10-8.21 parts per million (ppm) while these values are determined to be about 5.43-8.53 ppm and 5.38–8.50 ppm at B3LYP/6-311++G(d,p) and HF/6-311++G(d,p) calculation level, respectively. It is mentioned to be here that whereas all the data computed from the quantum chemical methods are found to be in good agreement with the experimental evidences, the results evaluated from the B3LYP/6-311++G(d,p) level of theory are noted to be superior to those from the other. Namely, the correlation between the theoretical results and experimental findings is found to be about 0.988 and 0.907 for the former and latter methods, respectively. Further, according to the results obtained, the greatest differentiation between experimental and theoretical data in the ^{1}H chemical shifts is noted to be about 1.29 and 1.73 ppm for the H_{22} and H_{35} atoms at B3LYP/6-311++G(d,p) and HF/6-311++G(d,p) level of calculation, respectively.

This difference stems from the atomic positions of the H_{35} and H_{22} atoms, meaning that the chemical shift may be more susceptible to intermolecular interactions in the aqueous solutions as compared to the other hydrogen atoms. It is another probable result that among the ^{1}H isotropic chemical shifts calculated, the H_{10} proton has the maximum chemical shift of 8.50 ppm for HF/6-311++G(d,p) level and H_{36}(8.53 ppm) for B3LYP/6-311++G(d,p) level because of the closer to the oxygen atoms in the monomer.

Furthermore, one can see the ^{13}C isotropic chemical shifts belonging to the BPOCPA in the table 8. The ^{13}C chemical shift values are found at 116.5–194.6 ppm 106.7–190.2 ppm at B3LYP/6-311++G(d,p) and HF/6-311++G(d,p) calculation level, respectively. Of the ^{13}C isotropic chemical shifts, the maximum chemical shift of 190.2 (194.6) ppm is observed for the C_{24} atom due to the bonding with the oxygen atom between the benzene rings in the monomer.

Table 7. Experimental and theoretical ^{1}H chemical shifts in BPOCPA

Nucleus	**Exp.**	**HF/6-311++G(d,p)**	**DFT/6-311++G(d,p)**
H_{10}	7.45	8.500	7.07
H_{23}	7.50	8.428	6.86
H_{8}	7.76	8.349	8.01
H_{9}	7.76	8.030	7.58
H_{21}	7.86	7.786	7.42
H_{36}	8.21	7.313	8.53
H_{20}	7.50	6.748	6.65
H_{33}	7.57	6.737	6.63
H_{22}	7.86	6.650	6.57
H_{32}	7.68	6.646	6.50
H_{7}	7.45	6.597	6.47
H_{35}	8.21	6.483	8.47
H_{34}	7.68	6.466	6.41
H_{43}	6.60	6.254	6.09
H_{42}	6.10	5.574	5.52
H_{44}	6.45	5.383	5.43

Table 8. Theoretical ^{13}C chemical shifts in BPOCPA

Nucleus	HF/6-311++G(d,p)	DFT/6-311++G(d,p)
C_{24}	190.205	194.64
C_{11}	160.141	163.34
C_{38}	159.762	163.12
C_1	151.083	159.07
C_{19}	149.202	157.41
C_5	130.561	140.35
C_{30}	130.374	135.47
C_3	129.85	133.28
C_{41}	128.631	133.14
C_{17}	127.854	133.05
C_{15}	127.139	132.40
C_{27}	124.549	131.12
C_{16}	124.368	130.48
C_{31}	123.734	129.69
C_{29}	123.511	129.15
C_{26}	120.092	128.22
C_{28}	118.05	126.62
C_{40}	113.446	126.16
C_4	112.266	124.28
C_{14}	111.33	119.48
C_2	109.801	119.18
C_6	107.111	117.80
C_{18}	106.659	116.51

4.3. Conclusion

In this study, we try to characterize the title compound, p-benzophenoneoxycarbonylphenyl acrylate (BPOCPA), with the aid of the experimental and theoretical investigations for the first time. Fourier transformation-infrared spectra, nuclear magnetic resonance chemical shifts, and ultra violet-visible (UV–vis) spectra measurements are performed for the experimental investigations when the theoretical examinations are composed of the optimized molecular structures, vibrational frequencies including infrared intensities and Raman activities, corresponding vibrational spectra, atomic charges, thermodynamic properties, UV–vis spectra, ^{1}H and ^{13}C NMR chemical shift values determined by ab initio Hartree–Fock (HF) and the density functional theory (B3LYP) with the standard 6-

311++G(d,p) calculation level in the ground state. Theoretical vibrational spectra are also interpreted by means of normal coordinate analysis based on scaled density functional force field. It is found that the computed vibrational frequencies, absorption wavelengths and chemical shifts (especially calculated form DFT/B3LYP) are in good agreement with the experimental findings for the title compound. The comparison between experimental evidences and theoretical results confirms that the calculation levels preferred are powerful approaches to understand the identification of the BPOCPA molecule studied in this work. Additionally, not only the frontier molecular orbitals (HOMO and LUMO), molecular electrostatic potential and electrostatic potential with total charge density contour are simulated but the dipole moment, softness, electronegativity, chemical hardness, electrophilicity index, transition state and optical energy band gap values are also analyzed seriously and the major conclusions to be obtained from this work are as follows:

- Thermodynamic investigations give that the title compound with higher polarity (non-uniform distribution of charges on the various atoms) is suitable to bond metallically.
- According to the atomic charge analysis, all the hydrogen atoms in the molecules lose electrons whereas all the oxygen atoms in the monomer accept electrons. Besides, carbon atomic charges are found to be both positive and negative values according to the position in the title compound. Based on the results obtained, the charge is transferred from hydrogen to carbon atoms.
- Uv-vis spectra results show that the absorption bands belonging to the BPOCPA molecule are experimentally centered at 310, 344 and 368 nm in the solution of THF. The absorption wavelength λ_{max} is observed at 344 nm due to the

effective π–π* conjugated segments in the title compound such as the C=C and vinylic group. The theoretical results indicate that the peak calculated in 344 nm (highest intense) corresponds to the overlapping of π-π* transition in benzene ring and oscillation effect whereas the weak absorption peak at 368 nm (smallest intense) stems from the $n \rightarrow \pi^*$ type transition in the carbonyl groups.

- The calculation results for the absorption bands are found to be shorter than the experimental evidences (blue shift) as a consequence of the calculations to be performed in the gas phase without considering the solvent effect.

- The NMR spectra results illustrate that the ^{1}H-NMR calculations obtained at B3LYP/6-311++G(d,p) level of theory are in better agreement with the experimental findings as compared to those of HF/6-311++G(d,p) basis set. This may be associated with the fact that no electron correlation effects are taken into account in HF methods whereas the B3LYP methods including the electron correlation effect treat the electronic energy as a function of the electron density of all the electrons in the material simultaneously.

- The largest differentiation between experimental and theoretical data in the ^{1}H chemical shifts is noted to be about 3 and 2 ppm for the H(5) atom at B3LYP/6-311++G(d,p) and HF/6-311++G(d,p) levels of calculation, respectively. This difference stems from the atomic position of the H(5), meaning that the chemical shift may be more susceptible to intermolecular interactions in the aqueous solutions as compared to the other hydrogen atoms. Moreover, among the ^{1}H isotropic chemical shifts, the OH proton (H_{12}) has the maximum chemical shift of 13.75 ppm due to the closer to the oxygen atoms in the monomer.

- Similarly, of the ^{13}C isotropic chemical shifts, the maximum chemical shift of 13.75 ppm is observed for the C_{12} atom due to the closer to the oxygen atoms in the

monomer.

- The frontier molecular orbitals (HOMO, and LUMO), molecular electrostatic potential (MEP) and electrostatic potential (ESP) simulated present that the BPOCPA molecule with the specific regions is useful to bond metallically and interact intermolecularly. Moreover, the electronegativity, hardness, softness and electrophilicity index calculated demonstrate that the monomer synthesized may be functional in the optic and opto-electronic applications.

REFERENCES

[1] C.M. Spillmann, J. Naciri, G. P. Anderson, M. S. Chen, B. R. Ratna, ACS Nano. 3 (2009) 3214–3220.

[2] O. Tongcher, R. Sigel, K. Landfester, Langmuir 22 (2006) 4504–4511.

[3] M. Vennes, R. Zentel, M. Rossle, M. Stepputat, U. Kolb, Adv. Mater. 17 (2005) 2123–2127.

[4] Z. Yang, W.T.S. Huck, S.M. Clarke, A.R. Tajbakhsh, E.M. Terentjev, Nat. Mater. 4 (2005) 486–490.

[5] C.M. Spillmann, J. Naciri, K.J. Wahl, Y.H. Garner III, M.-S. Chen, B.R. Ratna, Langmuir 25 (2009) 2419–2426.

[6] M. Eich, J.H. Wendorff, B. Reck, H. Ringsdorf, Makromol. Chem. Rapid. Commun. 8 (1987) 59–63.

[7] K. Anderle, R. Birenheide, M. Eich, J.H. Wendorff, Makromol. Chem. Rapid Commun. 10 (1989) 477–483.

[8] C. Griffin, A.M. Bhatti, R.S.L. Hung, "*In Non- Linear Optical and Electroactive Polymers*", Plenum, New York, 1988.

[9] C. Ravikumar, I.H. Joe, V.S. Jayakumar, Chem. Phys. Lett. 460 (2008) 552–558.

[10] Y.X. Sun, Q.L. Hao, L.D. Lu, X. Wang, X.J. Yang, Spectrochim. Acta A 75 (2010) 203–211.

[11] C.Y. Panicker, H. Varghese, L. Ushakumari, T. Ertan, I. Yildiz, C.M. Granadeiro, H.I.S. Nogueira, Y.S. Mary, J. Raman Spectrosc. 41 (2010) 381–390.

[12] L. Ushakumari, H.T. Varghese, C.Y. Panicker, T. Ertan, I. Yidiz, J. Raman Spectrosc. 39 (2008) 1832–1839.

[13] H.A. Dabbagh, A. Teimouri, A.N. Chermahini, M. Shahraki, Spectrochim. Acta A 69 (2008) 449–459.

[14] R.E. Hummel, "*Electronic Properties of Materials",* Springer Verlag, USA, 1992.

[15] A.K. Rappe, C.J. Casewit, *"Molecular Mechanics Across Chemistry",* University Science Book, USA, 1996.

[16] T. Yaman, Ms. Thesis, Gazi University, Ankara, 2011.

[17] S. Kecel, A.E. Ozel , S. Akyuz , S. Celik , G. Agaeva , J. Mol. Struct. 993 (2011) 349–356.

[18] J.B. Foresman, A.E. Frısch, "*Exploring Chemistry with Electronic Structure Methods"*, Gaussian, Pittsburgh, 1995-96.

[19] B.H. Bransden, C. J. Joachim, *"Physics of Atom and Molecules"*, Logman, London, 1983.

[20] Mc. Querrie, Donald A. "*Quantum Chemistry",* 2nd ed. University Science Books, United Kingdom, 2008.

[21] V. Kucuk, Phd. Thesis, Suleyman Demirel University, Isparta, 2009.

[22] H. Gokce, Ms. Thesis, Suleyman Demirel University, Isparta, 2009.

[23] U. Kara, Ms. Thesis, Suleyman Demirel University, Isparta, 2010.

[24] S. Erkoc, T. Uzer, *"Atomic and Molecular Physics", World Scientific Publishing, London, 1996.*

[25] J.R. Cheeseman, M.J. Frisch, F.J. Devlin, P.J. Stephens, J. Phys. Chem. A 104 (2000) 1039–1046.

[26] F.P. Miller, A.F. Vandome, J. McBrewster, *"Linear Combination of Atomic Orbitals Molecular Orbital Method",* Alphascript publishing, 2010.

[27] R.G. Parr, W. Yang, *"Density Functional Theory of Atoms and Molecules",* Oxford, 1989.

[28] K. Capelle, Braz. J. Phys. 36 (2006) 1318–1343.

[29] R. Dreizler, E. Gross, "*Density Functional Theory"*, Plenium, New York, 1995.

[30] W. Kohn, A.D. Becke, R.G. Parr, J. Phys. Chem. 100 (1996) 12974–12980.

[31] P. Hohenberg, W. Kohn, Phys. Rev. 136 (1964) B864–B871.

[32] A.D. Becke, "*In The Challenge of d and f Electrons: Theory and Computation"*, American Chemical Society, Washington, 1989.

[33] C. Lee, W. Yang, R.G. Parr. Phys. Rev. B 37 (1988) 785–789.

[34] A.D. Becke, J. Chem. Phys. 98 (1993) 1372–1377.

[35] J.P. Perdew, "*In Electronic Structure of Solids*", Akademie Verlag, Berlin, 1991.

[36] S.F. Boys, "*Electronic wave functions. I. A general method of calculation for the stationary states of any molecular system*", Proceedings of the Royal Society, London, 1950.

[37] D. Paschoal, B.L. Marcial, J.F. Lopez, W.B. Almeida, J. Comput. Chem. 33 (2012) 2292–2302.

[38] C.A. Barboza, P.A.M. Vazguez, D.M. Carey, R. Arratia-Perez, Int. J. Quantum Chem. 112 (2012) 3434–3438.

[39] P.W. Atkins, *"Quanta: A Handbook of Concepts",* Clarendon Press, London, 1974.

[40] R. Messerschmidt, M. Harthcock, "*Infrared Microspectroscopy: Theory and Applications*", Marcel Dekker, New York, 1988.

[41] D. Bougeard, M. Buback, A. Cao, K. Gerwert, H. M. Heise, G. G. Hoffmann, B. Jordanov, W. Kiefer, E. H. Korte, H. Kuzmany, A. Leipertz, E. Lentz, J. Liquier, A. Roseler, H. Schnockel, B. Schrader, H. W Schrotter, M. Spiekermann, E. Taillandier, H. Willner, "*Infrared and Raman Spectroscopy Methods and Applications*", VCH, New York, 1995.

[42] Inonu University, "*Fen ve Muhendıslık Bılımleri ıcın Enstrumental analiz*", Chemistry Publishings, Malatya, 2010.

[43] M. Balci, "Basic 1H- and 13C-NMR Spectroscopy", Elsevier Science, United Kingdom, 2005.

[44] D.A. Skoog, F.J. Holler, S.R. Crouch, *"Principles of Instrumental Analysis"*, Davit Haris, Canada, 1998.

[45] R.M. Silverstein, F.X. Webster, D. Kiemle, *"Spectrometric Identification of Organic Compounds"*, John Wiley & Sonsi Inc., USA, 2005.

[46] A.V.S. Sainath, A.K. Rao, A.V.R. Reddy, J. Appl. Polym. Sci. 75 (2000) 465–474.

[47] A.V.S. Sainath, T. Inoue, K. Yonetaka, K. Koyama, Polymer 24 (2001) 9859–9862.

[48] M.J. Frisch, G.W. Trucks, H.B. Schlegel, G.E. Scuseria, M.A. Robb, J.R. Cheeseman, G. Scalmani, V. Barone, B. Mennucci, G.A. Petersson, H. Nakatsuji, M. Caricato, X. Li, H.P. Hratchian, A.F. Izmaylov, J. Bloino, G. Zheng, J.L. Sonnenberg, M. Hada, M. Ehara, K. Toyota, R. Fukuda, J. Hasegawa, M. Ishida, T. Nakajima, Y. Honda, O. Kitao, H. Nakai, T. Vreven, J.A. Montgomery Jr., J.E. Peralta, F. Ogliaro, M. Bearpark, J.J. Heyd, E. Brothers, K.N. Kudin, V.N. Staroverov, R. Kobayashi, J. Normand, K. Raghavachari, A. Rendell, J.C. Burant, S.S. Iyengar, J. Tomasi, M. Cossi, N. Rega, J.M. Millam, M. Klene, J.E. Knox, J.B. Cross, V. Bakken, C. Adamo, J. Jaramillo, R. Gomperts, R.E. Stratmann, O. Yazyev, A.J. Austin, R. Cammi, C. Pomelli, J.W. Ochterski, R.L. Martin, K. Morokuma, V.G. Zakrzewski, G.A. Voth, P. Salvador, J.J. Dannenberg, S. Dapprich, A.D. Daniels, O. Farkas, J.B. Foresman, J.V. Ortiz, J. Cioslowski, D.J. Fox, *Gaussian 09*, Revision A.02, Gaussian, Inc., Wallingford, CT, 2009.

[49] R. Dennington II, T. Keith, J. Millam, *GaussView*, Version 4.1.2, Semichem, Inc., Shawnee Mission, KS, 2007.

[50] A.D. Becke, J. Chem. Phys. 98 (1993) 5648–5652.

[51] T. Schwabe, S. Grimme, Phys. Chem. Chem. Phys. 8 (2006) 4398–4401.

[52] A. Saiardi, H. Erdjument-Bromage, A.M. Snowman, P. Tempst, S.H. Snyder, Curr. Biol. 9 (1999) 1323–1326.

[53] M.J. Schell, A.J. Letcher, C.A. Brearley, J. Biber, H. Murer, R.F. Irvine, FEBS Lett. 461 (1999) 169–172.

[54] P. Pulay, G. Fogarasi, G. Pongor, J.E. Boggs, A. Vargha, J. Am. Chem. Soc. 105 (1983) 7037–7047.

[55] G. Rauhut, P. Pulay, J. Phys. Chem. 99 (1995) 3093–3100.

[56] G. Fogarasi, P. Pulay, "*In Vibrational Spectra and Structure"*, Elsevier, Amsterdam, 1985.

[57] G. Fogarasi, X. Zhou, P.W. Taylor, P. Pulay, J. Am. Chem. Soc. 114 (1992) 8191–8201.

[58] M.H. Jamroz, *Vibrational Energy Distribution Analysis: VEDA 4 program*, Warsaw, Poland, 2004.

[59] P.L. Polavarapu, J. Phys. Chem. 94 (1990) 8106–8112.

[60] G. Keresztury, S. Holly, J. Varga, G. Besenyei, A.Y. Wang, J.R. Durig, Spectrochim. Acta A 49 (1993) 2007–2026.

[61] P. Thanikaivelan, V. Subramanian, J.R. Raghava, B.U. Nair, Chem. Phys. Lett. 323 (2000) 59–70.

[62] R.G. Parr, R.G. Pearson, J. Am. Chem. Soc. 105 (1983) 7512–7516.

[63] P. Politzer, F.A. Awwad, Theor. Chem. Acc. 99 (1998) 83–87.

[64] P.W. Atkins, R.S. Friedman, "*Molecular Quantum Mechanics"*, 4th ed., Oxford University, USA, 2005.

[65] E.B. Wilson, J.C. Decius, P.C. Cross, "*Molecular Vibrations"*, Dover, New York, 1980.

[66] C.S. Hiremath, G.B. Kalkoti, M.K. Aralakkanavar, Spectrochim. Acta A 74 (2009) 200–204.

[67] S. Samdal, T.G. Strand, M.A. Tafipolsky, L.V. Vilkov, M.V. Popik, H.V. Volden, J. Mol.Struct. 435 (1997) 89–99.

[68] A.P. Scott, L. Radom, J. Phys. Chem. 100 (1996) 16502–16513.

[69] J.P. Merrick, D. Moran, L. Radom, J Phys Chem A 111 (2007) 11683–11700.

[70] J. Coates, "*Interpretation of Infrared Spectra: A Practical Approach, Encyclopedia of Analytical Chemistry",* Wiley, Chichester, 2000.

[71] P.G.N. Roeges, "*A Guide to Complete Interpretation of Infrared Spectra of Organic Structures"*, 1st ed., Wiley, New York, 1994.

[72] T.D. Klots, W.B. Collier, Spectrochim. Acta A 51 (1995) 1291–1316.

[73] L.J. Bellamy, "*The Infrared Spectra of Complex Molecules"*, 3rd ed., Wiley, New York, 1975.

[74] L. Rimai, M.E. Heyde, D. Gill, J. Am. Chem. Soc. 95 (1973) 4493–4501.

[75] M. Snehalatha, C. Ravikumar, N. Sekhar, V.S. Jayakumar, I.H. Joe, J. Raman Spectrosc. 39 (2008) 928–936.

[76] H.M. Badawi, J. Mol. Struc. (Theochem) 617 (2002) 9–15.

[77] G. Yildirim, S.D. Senol, M. Dogruer, O. Ozturk, A. Senol, A.T. Tasci, C. Terzioglu, Spectrochim. Acta A 85 (2012) 271– 282.

[78] O. Prasad, L. Sinha, N. Misra, V. Narayan, N. Kumar, J. Mol. Struct. 940 (2010) 82–86.

[79] I. Fleming, "*Frontier Orbitals and Organic Chemical Reactions",* Wiley, London, 1976.

[80] G. Gece, Corros. Sci. 50 (2008) 2981–2992.

[81] K. Fukui, Theory of Orientation, Stereoselection, 1st ed., Springer-Verlag, Berlin, 1975.

[82] H. Buyukuslu, M. Akdogan, G. Yildirim, C. Parlak, Spectrochim. Acta A 75 (2010) 1362–1369.

[83] D.F.V. Lewis, C. Ioannides, D.V. Parke, Xenobiotica. 24 (1994) 401–408.

[84] X.F. Zhang, H.B. Yu, Y.J. Xiao, Org. Chem. 77 (2012) 669–673.

[85] H. Ringsdorf, H.W. Schmidt, Makromol. Chem. 185 (1984) 1327–1334.

[86] M. Lewin, M. Jaffe, J.H. Wendorff, E. Tsuchida, "Polymers for Advanced Technologies", Wiley, New York, 1992.

[87] U. Wiesner, N. Reynolds, C. Boeffel, H.W. Spiess, Liq. Cryst. 11 (1992) 251–267.

[88] N. Ozdemir, B. Eren, M. Dincer, Y. Bekdemir, Mol. Phys. 108 (2010) 13–24.

[89] P. Politzer, J.S. Murray, Theor. Chem. Acc. 108 (2002) 134–142.

[90] F.J. Luque, J.M. Lopez, M. Orozco, Theor. Chem. Acc. 103 (2000) 343–345.

[91] N. Okulik, A.H. Jubert, Internet Electron. J. Mol. Des. 4 (2005) 17–30.

[92] C. Parlak, M. Akdogan, G. Yildirim, N. Karagoz, E. Budak, C. Terzioglu, Spectrochim. Acta A 79 (2011) 263–271.

[93] D.A. Dhas, I.H. Joe, S.D.D. Roy, T.H. Freeda, Spectrochim. Acta A 77 (2010) 36–44.

[94] S. Cetin, G. Yildirim, C. Parlak, M. Akdogan, C. Terzioglu, Spectrochim. Acta A 79 (2011) 1024–1033.

[95] R. Bauernschmitt, R. Ahlrichs, Chem. Phys. Lett, 256 (1996) 454–464.

[96] F. Furche, R.J. Ahlrichs, Chem. Phys. 117 (2002) 7433–7447.

[97] G. Yildirim, Y. Zalaoglu, C. Kirilmis, M. Koca, C. Terzioglu, Spectrochim. Acta A 81 (2011) 104–110.

[98] D. Sholl, J.A. Steckel, "*Density Functional Theory"*, John Wiley & Sons. Inc, Canada, 2009.

[99] L.J. Sham, M. Schlüterr, Phys. Rev. Lett. 51 (1983) 1888–1891.

[100] M. Karabacak, Z. Cinar, M. Cinar, Spectrochim. Acta A 85 (2012) 241–250

[101] J. Olsen, P.J. Jørgensen, Chem. Phys. 82 (1985) 3235–3264.

[102] T.U. Helgaker, H.J.A. Jensen, P.J. Jørgensen, Chem. Phys. 84 (1986) 6280–6284.

[103] V. Arjunana, S. Thillai Govindarajab, S. Sakiladevic, M. Kalaivania, S. Mohand, Spectrochim. Acta A 84 (2011) 196–209.

[104] G. Fitzgerald, J. Andzelm, J. Phys. Chem. 95 (1991) 10531–10534.

[105] D. Avci, Y. Atalay, M. Sekerci, M. Dincer, Spectrochim. Acta A 73 (2009) 212–217.